Nuclear Instruments and Methods in Physics Research A 368 (1996) 675–697

NUCLEAR INSTRUMENTS & METHODS IN PHYSICS RESEARCH Section A

ELSEVIER

ISOLTRAP: a tandem Penning trap system for accurate on-line mass determination of short-lived isotopes

G. Bollen [a,*], S. Becker [b,1], H.-J. Kluge [a], M. König [a], R.B. Moore [c], T. Otto [b,2], H. Raimbault-Hartmann [b,3], G. Savard [b,4], L. Schweikhard [b], H. Stolzenberg [b], the ISOLDE Collaboration [d]

[a] *Gesellschaft für Schwerionenforschung, Postfach 110552, D-64220 Darmstadt, Germany*
[b] *Johannes Gutenberg-Universität Mainz, Institut für Physik, D-55099 Mainz, Germany*
[c] *Foster Radiation Laboratory, McGill University, Montreal, PQ, H3A 2B1, Canada*
[d] *CERN, CH-1211 Geneva 23, Switzerland*

Received 12 May 1995

Abstract

The tandem Penning trap mass spectrometer ISOLTRAP has been set up at the on-line mass separator ISOLDE at CERN/Geneva for accurate mass measurements of short-lived nuclei with $T_{1/2} \geq 1$ s. The mass measurement is performed via the determination of the cyclotron frequency of an ion in a magnetic field. The design of the spectrometer matches the particular requirements for on-line mass measurements on short-lived isotopes. With the ISOLTRAP spectrometer masses of more than 70 radioactive nuclei have so far been determined with resolving powers exceeding one million and an accuracy of typically 10^{-7}.

1. Introduction

One of the most fundamental pieces of information that can be obtained about an atomic nucleus is its mass. It is simply the sum of the masses of the constituent protons and neutrons minus their binding energies.

The atomic masses of the stable isotopes are very well known [1], but the accuracy of the known masses decreases rapidly for nuclei that are more and more unstable with respect to β decay. There is a strong demand from the nuclear physics community for very precise mass values for some specific isotopes and for a general extension of the mass measurements to very unstable nuclei. Accurate experimental mass values serve as a stringent test of nuclear models, help to improve such models for predictions of the nuclear properties of very unstable nuclei that cannot be produced, and can reveal general nuclear structure. Deviations of binding energies from the smooth trend given by simple liquid-drop models directly reveal nuclear shell structure. Mass differences between odd and even numbered nuclei show the strength of the pairing force. Departures from a smooth trend of the two-neutron separation energies between shell closures can reveal the onset of strong ground state deformations.

The mass values of most of the radioactive isotopes have been provided by the determination of the Q-values (overall energy balances) of nuclear reactions or decays. The measurement of mass differences in long decay chains linking an unknown isotope to a nucleus of known mass allows, in principle, the determination of the mass of a very unstable nucleus. However, this procedure suffers from the possible propagation of systematic errors and the need to know the nuclear level scheme of the original nucleus and all the product nuclei in the decay chain. The determination of the mass of an unstable nucleus from the Q-value of a reaction depends on the availability of a target and a projectile that will lead directly to the desired nucleus by a reaction in which the products can be observed and their kinetic energies determined. This is not the case for the majority of unstable nuclei, particularly for the very unstable nuclei which are of most interest.

Direct measurements of the masses of unstable nuclei were achieved for the first time in the 1970s when conventional magnetic mass spectrometers were put on-line with

* Corresponding author. Tel. +49 6159 712141, fax +49 6159 71 2901, e-mail bollen@vscn.gsi.de.

[1] Present address: iC-Haus GmbH, Am Kuemmerling 18, D-55294 Bodenheim, Germany.

[2] Present address: Institute de Physique Nucléaire, Université Catholique de Louvain, B-1348 Louvain-la-Neuve, Belgium.

[3] Present address: CERN, CH-1211 Geneva 23, Switzerland.

[4] Present Address: AECL Research, Chalk River Laboratories, Chalk River, Ontario, Canada.

SSDI 0168-9002(95)00561-7

accelerators, starting with measurements performed at the proton synchrotron PS [2] and at the on-line isotope separator ISOLDE, both at CERN [3–5]. This type of mass spectrometry is still successfully applied to unstable nuclei at Chalk River [6]. Here, observation of the radioactivity of the unstable nucleus is combined with the mass spectrometer measurements to resolve ambiguities as to the actual nucleus or, in the case of isomers, the nuclear state that is being observed. This ambiguity cannot be removed by the mass measurement itself because of the limited resolution of the spectrometer.

During recent years new techniques for direct mass measurements have been developed. Direct mass spectrometry on recoils from target or projectile fragmentation reactions has been performed with the time-of-flight spectrometers TOFI at LAMPF/Los Alamos [7–12] and SPEG at GANIL/Caen [13–15]. Since the recoil ions are investigated without any delay, these devices allow masses of very short-lived isotopes to be determined, but their application is restricted to light isotopes by the limited resolving power, typically 3000, and by the lack of appropriate particle identification schemes for heavy ions. Further time-of-flight mass measurements are planned at existing machines such as the GANIL cyclotrons [16] and the storage ring ESR at GSI/Darmstadt [17,18]. In the case of the ESR another technique has already been successfully applied. In this technique, the mass of stored ions was determined via a frequency analysis of the Schottky-signal of the circulating cooled beam of highly charged ions [19].

Since the late 1940s static electric and magnetic fields have been employed to confine charged particles into small volumes within what is now being called a Penning trap and to determine the mass of these trapped particles by their cyclotron frequency $\omega_c = (q/m)B$ (q, B and m denoting respectively the charge, magnetic field and mass of the particle) [20]. Since then the methods have been refined and the Penning trap is becoming the instrument of choice for accurate mass measurements of charged particles. Mass measurements of very high accuracy have been demonstrated with experiments [21–28] performed on electrons, positrons, protons, antiprotons, ^{3}He and tritium ions, and ionized light molecules such as N_2 and CO. Except for the antiprotons, these experiments create or release the charged particles from material which is within or very close to the trap. Special techniques are applied such as, for example, narrow-band resonance detection via image currents and cooling by synchrotron radiation or by dissipating the ions' energy in cooled external resistive circuits. These techniques work efficiently only for light particles with high motional frequencies.

Besides their use for accurate mass determination, Penning traps are now being widely used in analytical chemistry, where their high resolving power for atomic masses can be used for accurate identification of large molecules. Mass identification in the ppm range has been achieved for broad mass ranges [29]. A higher accuracy is, in general, not needed for these applications. Therefore, stored ions can be driven to large motional amplitudes and the image currents of a large number of ions can be detected and Fourier-analyzed [30]. The technique is referred to as Fourier transform ion cyclotron resonance (FT-ICR).

A Penning trap mass spectrometer for the investigation of short-lived radioisotopes installed at an on-line mass separator has to fulfill a number of particular requirements. The ions to be investigated are delivered from an external (mostly continuous) source and have to be transferred into the trap used for mass determination. Generally, a retardation is required from some 10 keV energy of the delivered ion beam to almost thermal energies. The loading of the trap has to be as efficient as possible since the production rate for isotopes far from stability is generally very low and it is imperative to use the available beam time economically. The resonance detection scheme should cover a large mass range to allow fast switching between the masses to be determined and, in addition, should allow the detection of the motion of a single ion. In order to minimize systematic errors in the mass determination caused by trap imperfections, these imperfections must be minimized over as large a volume as possible. Finally, the ions must have kinetic energies as low as possible within the trap so as to reduce uncertainties due to disturbance of the resonance by the combined action of the thermal motion and imperfections of the electric and magnetic field.

We have developed and are further improving a tandem Penning trap system which meets these requirements. After construction and preliminary tests at Mainz, the ISOLTRAP spectrometer was set up at the ISOLDE-2 on-line mass separator at CERN in Geneva in 1986. Recently, ISOLTRAP has been moved to the new PS-Booster ISOLDE at CERN. In the following we give a description of the principles used in the ISOLTRAP spectrometer, the experimental setup, the experimental procedures and the performance of the present system. Improvements presently being carried out or to be added in the near future are briefly discussed in Ref. [31].

2. Principles of the ISOLTRAP spectrometer

In the ISOLTRAP spectrometer two Penning traps are used. One trap serves as ion collector, cooler and buncher and the second trap is used for the mass determination of stored ions via the determination of their cyclotron frequency. In the following the principle and the properties of a Penning trap will be explained as far as they apply to the ISOLTRAP spectrometer. For a more detailed description of the theoretical aspects concerning Penning traps see Refs. [32–36].

2.1. Ideal Penning trap

An ideal Penning trap can be defined as the superposition of a homogeneous magnetic field $\boldsymbol{B} = B\hat{z}$ and an electrostatic quadrupole field $U(\rho, z)$ coaxial to the magnetic

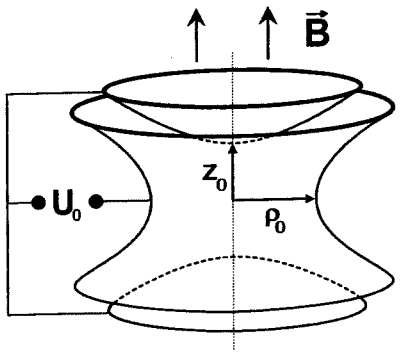

Fig. 1. Layout of a Penning trap. ρ_0 denotes the inner radius of the ring electrode and z_0 the half distance between the endcap electrodes.

field. The combination of these particular fields allows a charged particle to be stored in a well defined volume. Also, there is an exact solution of the particle's equations of motion. The electrostatic quadrupole field can be obtained by an electrode configuration as shown in Fig. 1, two endcaps and a ring electrode, all being hyperboloids of revolution and following the equipotential surfaces of the quadrupole field (ideally to infinity).

A potential difference U_0 (trapping potential) between the endcaps and the ring electrode creates the quadrupole potential

$$U(\rho, z) = \frac{U_0}{4d^2}(2z^2 - \rho^2). \tag{1}$$

The characteristic trap dimension d is determined by

$$4d^2 = (2z_0^2 + \rho_0^2), \tag{2}$$

where ρ_0 is the inner radius of the ring electrode and $2z_0$ the spacing between the endcaps.

The electric field causes the motion of a stored particle with mass m and charge q to deviate from pure cyclotron motion with frequency

$$\omega_c = \frac{q}{m}B \tag{3}$$

to become a superposition of three independent harmonic motions as illustrated in Fig. 2. These motions are an axial oscillation with frequency

$$\omega_z = \sqrt{\frac{qU_0}{md^2}} \tag{4}$$

and two radial motions. They are called the magnetron motion and the reduced cyclotron motion and have eigenfrequencies ω_- and ω_+, respectively, given by

$$\omega_\pm = \frac{\omega_c}{2} \pm \sqrt{\frac{\omega_c^2}{4} - \frac{\omega_z^2}{2}}. \tag{5}$$

From Eq. (5) it is easy to see that the sum of both radial eigenfrequencies is equal to the cyclotron frequency

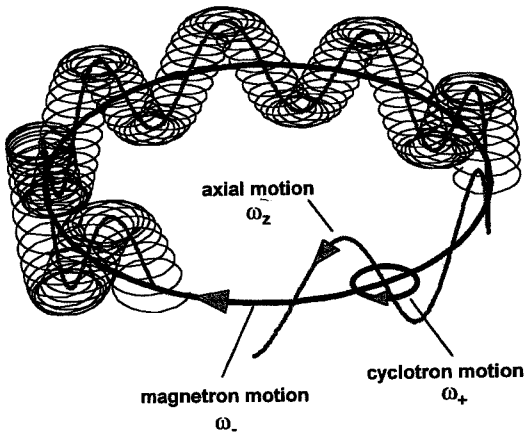

Fig. 2. Schematic of the three eigenmotions of an ion in a Penning trap.

$$\omega_c = \omega_+ + \omega_- \tag{6}$$

of an ion in a pure magnetic field. This is the most important equation in the context of the discussion of the ISOLTRAP spectrometer, since direct determination of this sum frequency allows a mass determination which depends only on the magnetic field B.

2.2. *Real Penning trap*

A real Penning trap will deviate from the ideal case as defined above in many aspects. Trap imperfections lead to shifts in the eigenfrequencies and to systematic errors in the mass determination. Knowledge of such imperfections and their influence is therefore essential for the design of a Penning trap mass spectrometer and for the understanding of possible systematic errors in the mass determination. The most important trap imperfections will be discussed briefly.

2.2.1. *Electric field imperfections*

Electric field imperfections are deviations from a pure quadrupole field as defined by Eq. (1). These imperfections arise from geometrical imperfections of the trap construction such as holes in the endcaps for injection or ejection of ions or from the unavoidable truncation of the electrodes. Deviations from the ideal field are commonly expressed in terms of a multipole expansion and the frequency shifts caused by octupole and dodecapole contributions have been calculated [32–34,36]. For the sum frequency $\omega_c = \omega_+ + \omega_-$ the frequency shift $\Delta\omega_c^{\text{elec}}$ depends on the amplitudes ρ_+, ρ_- and ρ_z of the cyclotron, the magnetron and the axial motion and is given by

$$\Delta\omega_c^{\text{elec}} = \Omega_c^{\text{elec}}\left[\frac{3}{2}\frac{C_4}{d^2}(\rho_-^2 - \rho_+^2) + \frac{15}{4}\frac{C_6}{d^4}(\rho_z^2(\rho_-^2 - \rho_+^2) - (\rho_-^4 - \rho_+^4))\right], \tag{7}$$

with

$$\Omega_c^{elec} = \frac{\omega_-}{1-\omega_-/\omega_+} \approx \omega_- \approx \frac{U_0/(2d^2)}{B}, \quad (8)$$

since, in general, $\omega_- << \omega_+$ and $\omega_- \approx (U_0/2d^2)/B$. C_4 and C_6 are, respectively, the coefficients of the octupole and dodecapole components of the electric field. From Eqs. (7) and (8) it can be seen that frequency shifts due to electrostatic field imperfections can be minimized by using a trap with large characteristic dimension d, by using small trapping potentials U_0 and by omitting or correcting for sources of higher multipoles (i.e. minimizing C_4 and C_6). Furthermore, the effect of imperfections can be reduced by using cold ions with small motional amplitudes ρ_+, ρ_- and ρ_z.

The frequency shift $\Delta\omega_c^{elec}$ is practically mass independent since Ω_c^{elec} is approximately mass independent. This type of frequency shift $\Delta\omega \neq f(m)$ always gives rise to calibration errors if a reference ion with mass m_{ref} is used for the determination of the magnetic field B via a cyclotron frequency measurement. The relative error in the mass determination of an ion with mass m_x and cyclotron frequency ω_x can be easily shown to be

$$\frac{\Delta m_x}{m_x} = \frac{\Delta\omega(m_x - m_{ref})}{\omega_x m_x} \propto m_x - m_{ref}. \quad (9)$$

When the highest accuracy is desired it is therefore advantageous to use mass doublets $m_{ref} \approx m_x$. On the other hand, ions with well known masses and a large mass difference can be used to examine residual trap imperfections.

Another source of frequency shift due to electric field imperfections arises from the image charge of the ion induced in the electrodes of the trap. Since these shifts scale inversely with the cube of the trap dimensions, considerable effects have to be expected for small traps [37]. If the sum frequency $\omega_+ + \omega_-$ is directly determined as in the case of ISOLTRAP, no frequency shift will be observed since $\Delta\omega_+ = -\Delta\omega_-$.

2.2.2. Misalignment

Another source of systematic errors in the mass determination is a tilting of the axis of the electrostatic trapping field with respect to the magnetic field axis [32]. Such a misalignment gives rise to shifts of all eigenfrequencies. For the sum frequency $\omega_c = \omega_+ + \omega_-$ the resulting shift $\Delta\omega_c^{tilt}$ can be calculated [33] and is found to be mass independent and, for $\Theta << 1$, to be proportional to the square of the tilting angle Θ [32]:

$$\Delta\omega_c^{tilt} \approx \tfrac{9}{4}\omega_- \sin^2\Theta. \quad (10)$$

Again, the frequency shift is mass independent and can cause systematic errors as described by Eq. (9). A careful alignment of the trap with respect to the magnetic field is therefore necessary.

2.2.3. Magnetic field imperfections

For accurate mass determinations via cyclotron resonances a high homogeneity and temporal stability of the magnetic field is required. Commercial superconducting magnets nowadays provide a homogeneity of typically $\Delta B/B < 10^{-8}$ over a volume of 1 cm^3 and a stability of the field of $(\Delta B/B)/\Delta T < 10^{-8}$/h. The homogeneity can be destroyed if material with a magnetic susceptibility is introduced into the magnetic field. Such material can be the components of the trap itself. The susceptibility of the materials commonly used in trap construction (typically oxygen-free high-conductivity copper and glass ceramics) is low. Nevertheless, the values are high enough to create a noticeable perturbation of the field.

Frequency shifts arise if the magnetic field is a function of even powers of the distance from the trap center [32,34]. A stored ion then experiences different average magnetic fields for different motional amplitudes. The lowest-order inhomogeneity of interest is a magnetic hexapole

$$B_2 = B\beta_2(\rho_z^2 - \rho^2/2), \quad (11)$$

where B is the value of the field at the center of the magnet and β_2 denotes the relative strength of the hexapole component. This field creates a frequency shift given by

$$\Delta\omega_c^{magn} \approx \beta_2\omega_c(\rho_z^2 - \rho_-^2). \quad (12)$$

Compared with the frequency shifts discussed above the shift is now proportional to the cyclotron frequency of the stored ion and does not give rise to a calibration error, provided the amplitudes of the motion of the two ion species are equal. Since this can only be achieved within certain limits, it is still important to construct the trap so that the inhomogeneity (i.e. β_2) is sufficiently small for the required accuracy in the mass determination.

Another point of concern is the stability of the magnetic field. As reported and discussed for a number of Penning trap experiments [23,38–40] the field stability is determined by the magnet itself, by changes in the ambient magnetic field, by pressure changes in the helium cryostat and temperature changes of the experimental equipment installed inside the bore of the magnet. The demand on the magnetic-field stability is determined by the desired accuracy and the time needed to switch between the cyclotron frequency measurements of the reference ion and the ion under investigation.

2.2.4. Storage of more than one ion

In ISOLTRAP, cyclotron frequency determinations are performed with typically a few tens of ions in the trap. Hence effects of Coulomb interactions on the ion motion have to be considered. In a number of experiments, effects resulting from Coulomb interactions have been observed and investigated for both the Penning [41–44] and the Paul trap [45]. They give a clear picture of the effects of these interactions on the cyclotron frequency which in the following is discussed in the context of a cyclotron frequency determination. If the simultaneously stored ions are equal in mass, a driving field acts on the q/m center of the cloud and no frequency shift is observed [46]. This is not so in the case

of two ion species differing in mass which are confined together. Such contaminations cause frequency shifts $\Delta\omega_c^{Cb}$ in the observed resonances. It was found [43] that the sign of $\Delta\omega_c^{Cb}$ depends strongly on the cyclotron frequency difference of the ions compared with the linewidth of the resonances. The size of the shift increases with the total number of stored ions. In the case when the unperturbed resonances cannot be resolved, one single resonance is observed, which is narrower than expected from a simple superposition. The position of this resonance corresponds to the average mass of all the ions in the trap. When there is a large mass difference between the two ion species, so that the unperturbed resonances are separated by more than their widths, the measured resonances are both shifted to lower frequencies. The size of the resonance shift for ions of one species is found to be proportional to the number of ions of the other species and vice versa.

A quantitative description of the observed frequency shifts must take into account the coupling of all eigenmotions by Coulomb interaction. Up to now no general analytical solution has been found for the equations of motion, neither for the Paul nor the Penning trap. Nevertheless, it was possible to confirm the experimental observations qualitatively by a three-dimensional simulation of the motions of simultaneously stored ions [43].

In practice, it is therefore necessary to have pure ion samples in the trap. If this is not possible a careful analysis of the frequency shifts as a function of the number of stored ions has to be performed, so that an extrapolation can be made to the cyclotron frequency of a single stored ion.

2.3. Excitation of stored ion motion and cyclotron resonance detection

In order to detect the cyclotron frequency of the stored ions, to remove unwanted ion species from the trap or to be able to use buffer gas cooling in a Penning trap it is necessary to drive the ion motion with oscillating electric fields. The effect of the driving field on the motion depends on the multipolarity of the field and its frequency.

With dipole fields the ion motions can be excited at their eigenfrequencies. In all cases an increase of the amplitudes of the eigenmotions is achieved (assuming zero initial amplitudes). A dipole field in the axial direction with frequency ω_z acts on the axial motion while an azimuthal dipole field with frequency ω_+ or ω_- drives the cyclotron or the magnetron motion, respectively. In the ISOLTRAP experiment the ω_+ excitation serves to remove unwanted ion species from the precision trap by increasing their cyclotron amplitude until they are lost.

A quadrupole field in general allows the excitation of two ion motions at the sum or difference of the eigenfrequencies. In ISOLTRAP, excitation by an azimuthal quadrupole field at a frequency of $\omega_+ + \omega_-$ is used for the direct determination of the true cyclotron frequency ω_c. In particular cases, excitation at $2\omega_+$ is used for the removal of unwanted ion species.

The required azimuthal quadrupole field is described by

$$E_x = \frac{2V_d}{a^2}\cos(\omega_d t)\,y,$$
$$E_y = \frac{2V_d}{a^2}\cos(\omega_d t)\,x, \qquad (13)$$

where V_d is the amplitude of the potential of the driving azimuthal quadrupole field at radius a and ω_d is the angular frequency of that driving field. (If a four-segmented ring electrode with inner radius $\rho_0 = a$ is used for the creation of the azimuthal quadrupole field, then V_d is to first order equal to the amplitude V_{RF} of the oscillating voltages applied to the ring segments.)

When $\omega_d = \omega_+ + \omega_-$ the field couples both radial plane eigenmotions so that an initially pure magnetron motion with amplitude $\rho_{-,0}$ is completely converted into a pure cyclotron motion with radius $\rho_+ = \rho_{-,0}$ [33,47] after a period T_{conv}, as illustrated in Fig. 3. The conversion time is

$$T_{conv} = \frac{m}{q}\frac{a^2}{2V_d}(\omega_+ - \omega_-)\pi = B\frac{a^2}{2V_d}\frac{\omega_+ - \omega_-}{\omega_c}\pi. \qquad (14)$$

A full conversion is therefore achieved with excitation time $T_{RF} = T_{conv}$. Continued excitation forces the motion to oscillate between a pure magnetron and a pure cyclotron motion with a period $2T_{conv}$. It should be noted that T_{conv} is, to first order ($\omega_+ - \omega_- \approx \omega_c$), mass independent and only dependent on the magnetic field B and the driving quadrupole potential V_d.

For detection of the cyclotron resonance the change in kinetic energy ΔE_r that accompanies a full conversion is important:

$$\Delta E_r = \frac{m}{2}(\omega_+^2 - \omega_-^2)(\rho_{-,0}^2 - \rho_{+,0}^2). \qquad (15)$$

In the ISOLTRAP spectrometer this energy gain is used for the detection of the cyclotron resonance. Therefore, it is desirable to have a finite magnetron amplitude $\rho_{-,0}$ and a vanishing cyclotron amplitude $\rho_{+,0}$ at the beginning of the excitation.

A full conversion in the time given by Eq. (14) is only achieved if $\omega_d = \omega_c$. The energy gained for the same strength and duration of the quadrupole field but at driving frequencies that are not equal to ω_c is given by [47]

$$E_r(\omega_d) = \frac{q^2V_d^2}{2ma^4}\frac{\omega_+^2}{(\omega_+ - \omega_-)^2}\frac{\sin^2(\omega_b T_{RF})}{\omega_b^2}, \qquad (16)$$

with

$$\omega_b = \tfrac{1}{2}\sqrt{(\omega_c - \omega_d)^2 + (\pi/T_{conv})^2}. \qquad (17)$$

Fig. 4 shows the resulting energy gain profile. The theoretical linewidth can be calculated to be

$$\Delta\nu(\mathrm{FWHM}) = (1/2\pi)\Delta\omega(\mathrm{FWHM}) \approx 0.8/T_{RF}. \qquad (18)$$

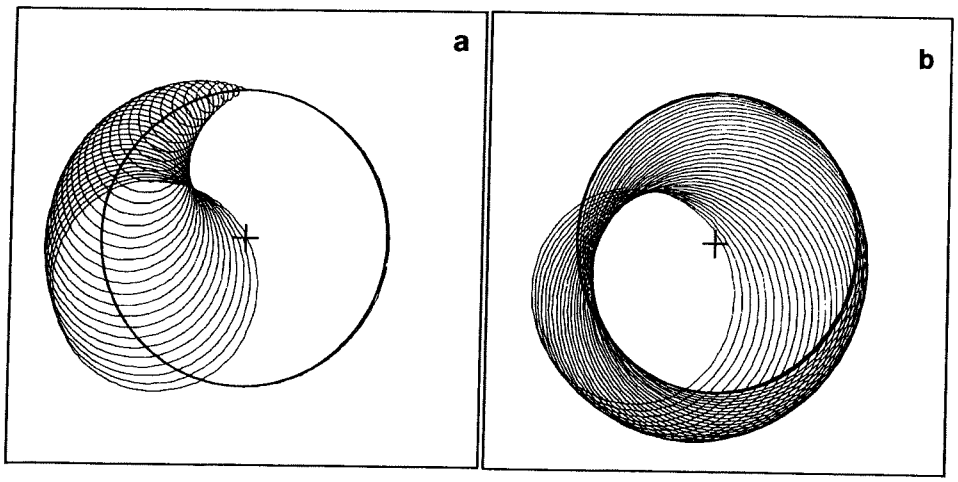

Fig. 3. Calculated ion trajectories in a plane perpendicular to the magnetic field. Shown is the development of the ion motion from an initial pure magnetron (a) to a pure cyclotron motion (b) if the ion is exposed to an azimuthal electric quadrupole field of frequency ν_c. In both frames the initial magnetron motion is indicated by a circle and the center of the trap by a cross.

It should be noted that, in the case of the conversion of a pure magnetron motion into a pure cyclotron motion, frequency shifts due to electric field imperfections cancel. According to Eq. (7) the ion will experience equal amounts of positive and negative shifts $\Delta\omega_c^{elec}$ during the conversion. A more detailed analysis [33] indeed confirms that the central peak of the cyclotron resonance curve is not shifted, but shows that the full resonance profile is asymmetric.

There exists a number of schemes for the detection of the eigenfrequencies of a trapped ion. Two that are widely used are narrow- and broad-band detection of the image currents induced in the trapping electrodes. However, these schemes are in general not applicable to unstable isotopes. The narrow-band detection technique with tuned circuits [22–24,26,46] has only a limited dynamic range for switching between different masses. Furthermore, a long storage time is required for a good signal-to-noise ratio if single-ion measurements are performed. Broad-band detection is used in FT-ICR experiments and has recently been applied in quadrupolar geometry to yield resonance signals at $\omega_c = \omega_+ + \omega_-$ [48,49]. However, it requires a large number of stored ions for a detectable signal, especially if the radii of the motions have to be kept small [30]. Therefore, some other technique that is simple, sensitive and universally applicable is needed for the investigation of short-lived heavy isotopes.

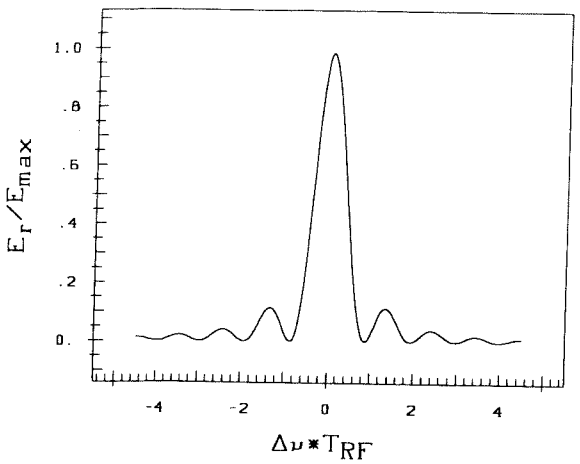

Fig. 4. Radial energy at the end of the application of an azimuthal quadrupole field as a function of the excitation frequency ν_{RF}. The field strength has been chosen so as to result in a full conversion of magnetron into cyclotron motion for $\nu_{RF} = \nu_c$ as illustrated in Fig. 3.

In ISOLTRAP the cyclotron resonance is detected via conversion of the cyclotron energy into axial energy in a magnetic field with a negative gradient [21]. This technique is based on the interaction of the magnetic moment of the ion orbit with the gradient of the magnetic field. After cyclotron excitation, the ions are ejected from the trap and allowed to drift along the magnetic field lines to an ion detector placed in the fringe field of the magnet. The magnetic moment of a trapped ion with cyclotron energy $E \approx E_r(\omega_d)$ in a magnetic field $\boldsymbol{B} = B\hat{z}$ is $\boldsymbol{\mu}(\omega_d) = [E_r(\omega_d)/B]\hat{z}$. If the ion motion through a varying magnetic field is slow, as it is in ISOLTRAP, the magnetic moment is preserved.

This magnetic moment and the magnetic field gradient cause the ion to experience an axial force $\boldsymbol{F}(\omega_d, z) = -\boldsymbol{\mu}(\omega_d) \cdot \nabla \boldsymbol{B}(z)$. This force increases the axial energy of the ions and leads to a reduction of the time of flight from the trap at position z_0 to the detector at position z_1. Including a variable electrostatic potential $U(z)$ along the flight path, the time of flight to the detector can be evaluated from

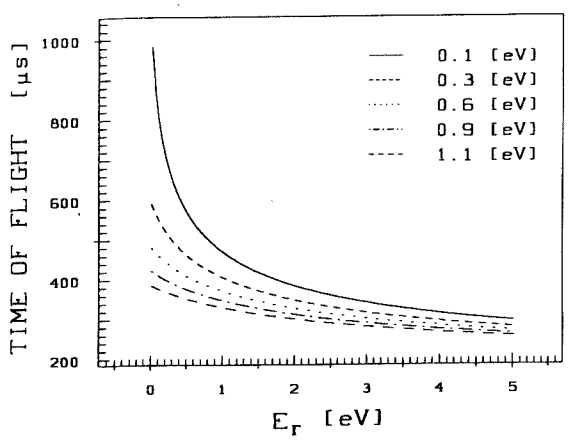

Fig. 5. Calculated time of flight of ions from a Penning trap to a detector in the fringe field as a function of the ions' radial energy for different initial axial energies. The calculation is based on the electric and magnetic field shown in Fig. 17.

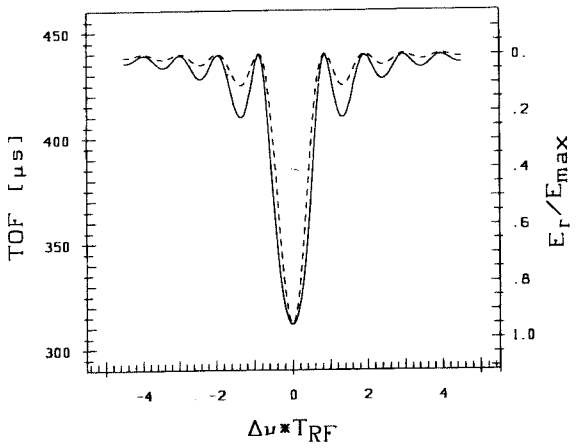

Fig. 6. Theoretical line shape of a cyclotron resonance as obtained from the energy gain shown in Fig. 4 and the transformation into time of flight (Fig. 5). For comparison, the line shape of the energy gain has been included (dotted line).

$$T(\omega_d) = \int_{z_0}^{z_1} \left[\frac{m}{2(E_0 - qU(z) - \mu(\omega_d)B(z))}\right]^{1/2} dz, \quad (19)$$

where E_0 is the total initial energy of the ion. The magnetic moment $\mu(\omega_d)$ reaches its maximum at $\omega_d = \omega_c$ resulting in a minimum time of flight. Fig. 5 shows the theoretical time of flight as a function of the initial radial energy E_r for an ion of mass number $A = 100$ with different axial kinetic energies E_z. The figure is based on the electric and magnetic fields and the configuration used in the ISOLTRAP spectrometer (see Section 3.3.3). For a given gain in radial energy the change in time of flight is largest for small initial axial energies. It is therefore important to eject the ions from the trap with a low initial axial energy.

As can be seen from the figure the conversion of radial energy into time of flight is not linear. Therefore, the experimentally observed line shape of a cyclotron resonance differs from the energy gain profile shown in Fig. 4. Combining the energy gain given by Eq. (16) with the conversion into time of flight (Eq. (19)) results in a theoretical line shape for the cyclotron resonance curve as shown in Fig. 6. For comparison, the energy absorption profile is also plotted. It can be observed that the non-linearity of the conversion gives rise to a slight increase of the linewidth of the central peak and an enhancement of the side peaks of the resonance.

2.4. *Buffer gas cooling in a Penning trap*

The most important task of cooling in traps is to decrease the amplitudes of the motions of the stored ion. Small amplitudes are needed in order to reduce the effects of trap imperfections on the measurements. The cooling techniques that have been developed for ion motion are resistive dissipation in a cooled external circuit via the image currents induced in the trap electrodes, interaction with an intense laser beam of appropriate wavelength, sympathetic cooling with cold charged particle clouds, and buffer gas cooling. For mass measurements on short-lived isotopes the first three techniques are not useful. The currents induced in an external circuit for resistive cooling [50] are proportional to the particle velocity and for heavy ions this is too low to achieve significant cooling in the time available. The technique works well only for light particles with high motional frequencies. Sub-Kelvin temperatures can be reached via laser cooling [51–53], but optical transitions of appropriate wavelength are required and therefore the applicability is limited to only a few particular ion species. This restriction can in principle be overcome by using laser-cooled ions for sympathetic cooling of another ion species [54,55], but effects due to the Coulomb interaction between both clouds modify the eigenmotions. Cooling with cold clouds of electrons [56], which cool themselves by synchrotron radiation, has successfully been applied to antiprotons, but cooling of ions with positrons has not yet been demonstrated.

The use of buffer gas collisions for the cooling of stored ions is a well established technique applied to Paul traps [50,57–62]. Here, the ion experiences a force directed towards the center of the trap for all directions of excursion of the ion from the trap center. However, in a Penning trap the magnetron motion is unbound. Simply removing energy from the three degrees of freedom causes the ion to migrate outward radially from the center of the trap. Introducing a velocity-dependent force $\boldsymbol{F} = -\gamma \boldsymbol{v}$ into the equations of motion results in time-dependent amplitudes for all three eigenmotions

$$\rho_z(t) = \rho_z^0 \, e^{-(\gamma/m)t/2},$$

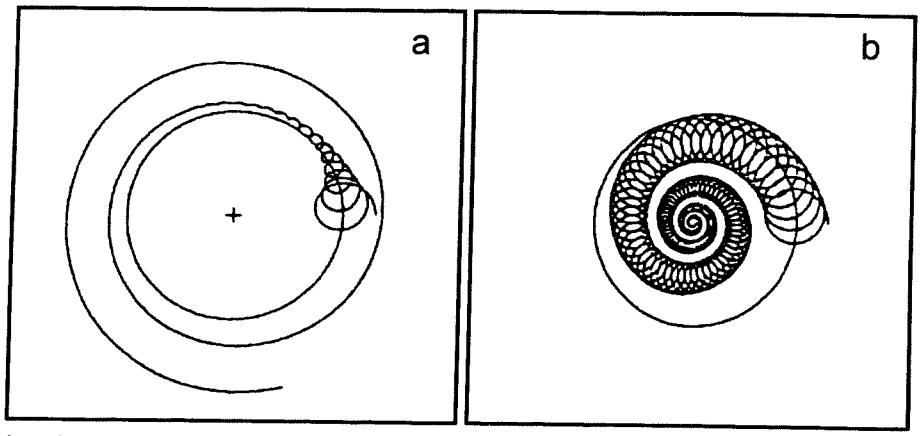

Fig. 7. Calculated ion trajectories in a plane perpendicular to the magnetic field. A damping force has been included in the equations of motion. On the left, a fast damping of the cyclotron motion and a slow increase of the magnetron motion are observed. On the right, the effect of an additional azimuthal quadrupole field of frequency ν_c is shown. Both cyclotron and magnetron motions are decreased.

$$\rho_{\pm}(t) = \rho_{\pm}^{0}\, e^{\mp\alpha_{\pm} t}, \tag{20}$$

with

$$\alpha_{\pm} = \frac{\gamma}{m}\frac{\omega_{\pm}}{\omega_{+} - \omega_{-}}. \tag{21}$$

The friction coefficient γ is inversely proportional to the ion mobility in the particular gas and proportional to the gas pressure [63]. As can be seen from Eq. (20) both the axial and the cyclotron motion are damped while the amplitude of the magnetron motion increases. This process can be circumvented by coupling the magnetron and cyclotron motions [33,47,64,65]. As in the scheme for cyclotron resonance detection (Section 2.3), this coupling is achieved by driving the ion motion with an azimuthal quadrupole field at $\omega_{+} + \omega_{-}$. In the long-term average both motions attempt to reach the same amplitude (see Fig. 3). However, due to its higher frequency the cyclotron motion is more strongly damped than the magnetron motion and therefore the amplitudes of both motions decrease exponentially as illustrated in Fig. 7. The time constant η for this centering process can be calculated and reaches its minimum $\eta_{\min} = -(1/2)(\gamma/m)$ for an amplitude of the driving field $2V_d/a^2 \geq (\gamma/m)B$ [47]. The centering process is mass selective since the cyclotron frequency $\omega_c = \omega_{+} + \omega_{-}$ is involved. This process results not only in the cooling of the ion species selected for measurement, but also in the removal of unwanted contaminants, which is favourable for accurate mass measurements.

3. Experimental setup of ISOLTRAP

The ISOLTRAP spectrometer was first installed at the on-line mass separator ISOLDE-2 at CERN, Geneva. Following the shut-down of ISOLDE-2 in 1990 the apparatus was installed without major modifications at the new CERN PS-Booster ISOLDE facility. Fig. 8 shows the schematic

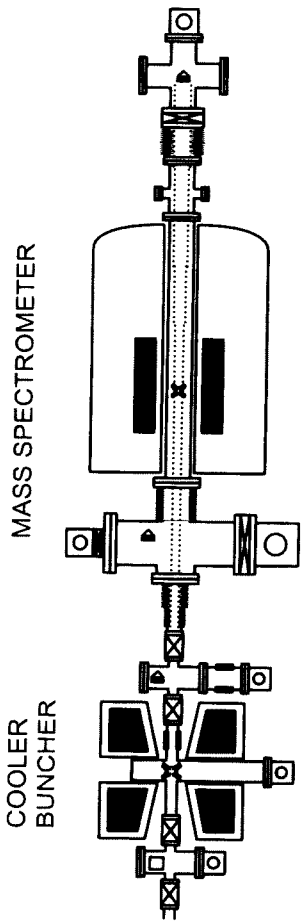

Fig. 8. Layout of the experimental setup of the ISOLTRAP mass spectrometer installed at ISOLDE/CERN. It consists of an ion beam buncher and cooler and a mass spectrometer section.

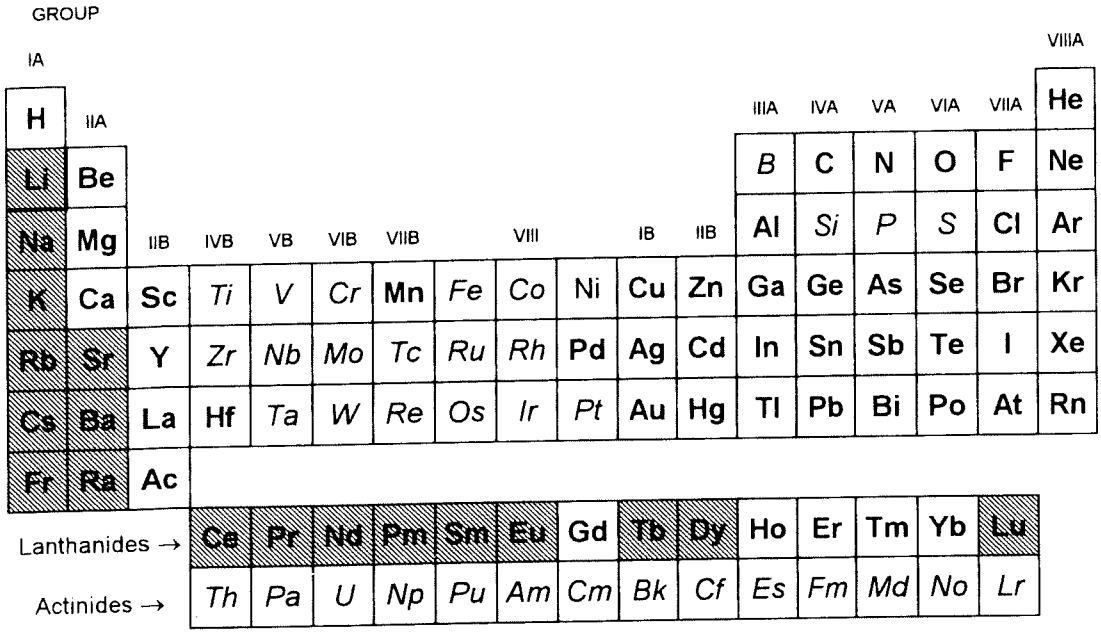

Fig. 9. Periodic table of the elements. Elements which can be delivered by ISOLDE are printed bold. Italic characters are used for those elements which cannot be produced. Elements which can presently be investigated by ISOLTRAP are shaded.

layout of the spectrometer. ISOLTRAP consists of two main components, a Penning trap ion buncher and cooler for the radioactive ions delivered by ISOLDE and a high-precision Penning trap for the mass determination. Recently, the buncher and cooler trap has been replaced by an improved version. It will not be described here, since modifications of the setup are still going on and the performance of the new system has not yet been fully tested. In the following the setup of ISOLTRAP, as it was operating until the beginning of 1994, will be discussed in detail, preceded by a short description of the ISOLDE facilities.

3.1. Production of radioactive isotopes at ISOLDE/CERN

The ISOLDE on-line isotope separators [66,67] at CERN/Geneva have led the world in the production of radioactive isotopes of a large number of different elements with high yields. At these facilities radioactive isotopes are produced via spallation or fission by bombarding suitable targets with light projectiles. In the now closed ISOLDE-2 either 600 MeV protons or 910 MeV $^3He^{2+}$ ions were delivered by the synchrocyclotron (SC). The new ISOLDE facility uses 1 GeV protons from the booster of the proton synchrotron (PS-Booster). The radioactive products diffuse from the target to an ion source and are ionized either by plasma or surface ionization. Ions extracted from the source are accelerated to 60 keV, mass separated in a magnetic sector field and sent to the experiments via different beam lines. The mass resolving power of the separator of the ISOLDE-2 facility was typically $R = 500$. With the new general purpose separator (GPS) at the new ISOLDE facility a value of $R = 2000$ has been achieved. Fig. 9 shows a periodic table where those elements which can be produced at ISOLDE are printed bold. Those elements which can presently be investigated with the ISOLTRAP spectrometer are shaded.

3.2. The ISOLTRAP ion cooler and buncher

The lower part of the ISOLTRAP spectrometer is for collecting ions delivered by ISOLDE or by a test ion source, cooling them via buffer gas collisions and finally sending them as a bunch to the mass spectrometer part of the apparatus. Fig. 10 shows schematically the layout of the ion cooler and buncher. The magnetic field of $B = 0.7$ T is provided by a conventional split coil electromagnet (BRUKER). A Penning trap (TRAP 1) is installed in the center of the magnetic field in a vacuum chamber between the two pole faces. The chamber below the magnet is connected to the ISOLDE beamline and contains a surface ionization source for stable rubidium and cesium ions. This source can be moved into the axis of the system and is used for tests of the apparatus and for the calibration of the magnetic field in the precision trap. The chamber above the magnet contains part of the ion optics used for the transport of the ion bunch and a microchannel plate ion detector (MCP 1) for tests of the cooler and buncher trap. All three chambers are pumped by turbomolecular pumps. The upper chamber is designed to provide efficient differential pumping. This is needed to remove the gas load from the trap chamber where buffer gas

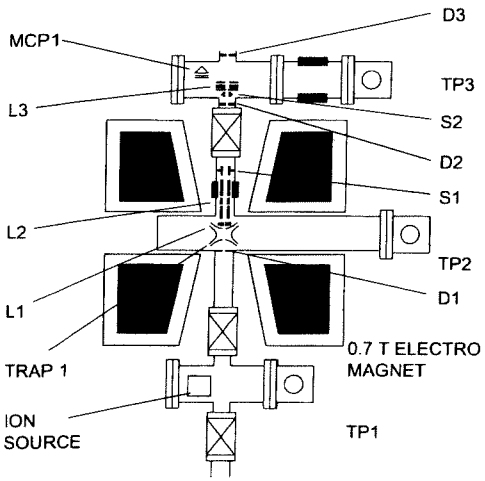

Fig. 10. Layout of the ion cooler and buncher (see Fig. 8). Only the most important elements are shown. L denotes electrostatic lenses, S deflectors, D diaphragms, MCP the ion detector and TP turbomolecular pumps.

is used.

Fig. 11 shows the design of the Penning trap of the cooler. A rotatable collector and surface ionizer are installed in the lower endcap. It consists of two holders for two rhenium filaments (3.5×6 mm^2, 20 μm thick) placed at 180° with respect to each other. The whole assembly can be turned by 180° from the outside of the vacuum chamber within 2 s by means of a servo motor. The foil pointing downwards is connected to a contact for measurement of the current of the incoming ion beam. In order to ensure that the ions from ISOLDE or the test ion source hit the center of the filament a diaphragm (D1) of 3 mm diameter is installed in the bottom of the trap chamber. The foil pointing upwards is connected to two contacts providing the heating current required for the release and surface ionization of the collected atoms. The temperature of the foil is monitored via an optical light guide and a photodiode placed behind a glass window outside the vacuum.

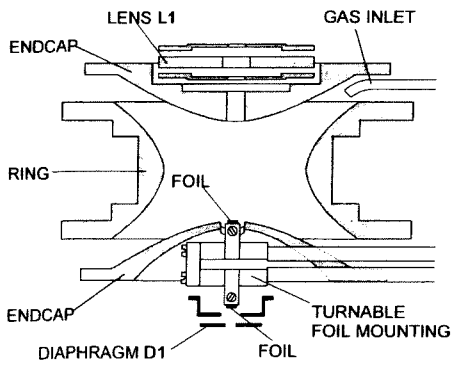

Fig. 11. The low-precision Penning trap used in the ion cooler and buncher (see Figs. 8 and 10).

Table 1
Dimensions and important parameters of the Penning trap (TRAP 1) used in the ion cooler and buncher

Trap characteristics	Low precision hyperbolic trap for collecting, cooling and bunching of ions delivered by the on-line mass separator ISOLDE	
Trap materials	Stainless steel, PTFE, ceramics	
Helium buffer gas pressure	p	10^{-3}–10^{-4} mbar
Trap dimensions	ρ_0	20.00 mm
	z_0	14.14 mm
	d	14.14 mm
Magnetic field	B	0.7 T
Potentials	Ring electrode	−10.0 V
	Endcaps	0.0 V
Eigenfrequencies of an ion with mass number $A = 100$	ν_+	101 kHz
	ν_-	6 kHz
	ν_z	35 kHz

For capture and cooling of the ions produced by surface ionization, buffer gas is leaked into the trap via a line connected to a needle valve outside the vacuum. The ring electrode of the trap is split into quadrants for the creation of the azimuthal quadrupole field needed for the mass selective centering of the ions as discussed in Section 2.4.

An ion bunch ejected from the trap can be accelerated to an energy of 1 keV by means of three diaphragms (L1) incorporated in the upper endcap. An einzel lens (L2) (see Fig. 10) and a pair of deflectors (S1) placed in the beam line connecting the trap chamber to the detector chamber deliver the ions through a 3 mm diaphragm (D2) needed for the differential pumping. Another einzel lens (L3) and a set of deflectors (S2) placed in the chamber above the electromagnet finally guide the ions through a diaphragm (D3) into the entrance slits of the mass spectrometer part of the apparatus. Dimensions and important parameters of the cooler and buncher trap are summarized in Table 1.

3.3. The mass spectrometer part of ISOLTRAP

The purpose of this part of the setup (Fig. 8) is to excite and detect the cyclotron resonance of ions transported to the precision trap. Fig. 12 gives an overview of the layout of the vacuum system and of the ion optical elements.

A superconducting magnet (OXFORD 250/89) provides a 6.0 T magnetic field for the precision trap. The magnet has a warm bore design with a bore diameter of 89 mm. It is equipped with superconducting shim coils in order to achieve a homogeneity of $< 10^{-7}$ T in a volume of 1 cm^3. The specified relative stability of the magnetic field is 10^{-8} per hour.

The vacuum enclosure for the ion optical parts consists essentially of three chambers, one below the superconducting magnet, a tube inside the bore of the magnet which contains the precision trap, and a detector chamber above the magnet. The chambers are connected with bellows in order to ease

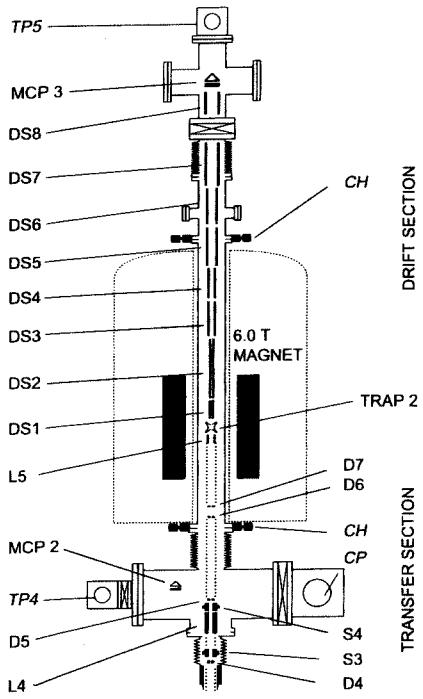

Fig. 12. Layout of the mass spectrometer part of ISOLTRAP consisting of a transfer section, the precision trap TRAP 2, and a drift section. L denotes electrostatic lenses, S steerers, D adjustable diaphragms, DS electrostatic elements in the drift section and MCP ion detectors. TP are turbomolecular pumps and CP a cryopump. CH denotes cardanic holders for the vacuum tube inside the bore of the magnet.

adjustment. All vacuum parts are made from stainless steel, the tube inside the magnet having been selected so as to have a low susceptibility and no magnetic enclosures. This tube, which is precisely machined inside, serves directly as the optical bench for all ion optical parts placed in it. The parts are mounted on 1 cm thick discs made from OFHC copper, which themselves fit into the tube within ±0.05 mm and therefore assure a good alignment of the optics. The tube itself is mounted in cardanic holders (CH) at both its ends. Micrometer screws allow a precise and reproducible positioning inside the bore of the magnet. An ultrahigh vacuum of $p < 10^{-8}$ mbar is achieved with turbomolecular pumps at both the lower (TP4) and the detector chamber (TP5) and an additional cryopump (CP) at the lower chamber.

The alignment of the vacuum tube inside the bore with the magnetic field axis was performed after a first shimming of the magnet and before the trap and additional ion optical parts were inserted. It was accomplished by means of an assembly consisting of an electron gun and a number of diaphragms and pin holes all mounted on discs with close tolerance fitting to the vacuum tube. The electron gun, which directs electrons in two directions, is a current heated filament with 0.2 mm pin holes on both sides aligned with the tube axis. About 25 cm above and below the gun, detectors are mounted that basically consist of a 0.4 mm pin hole in front of a plate insulated from electric ground. The whole assembly was inserted into the vacuum tube with the electron gun positioned in the center of the magnetic field. By tilting and shifting of the tube it was possible to have the electron current completely passing both detector pin holes. From the dimensions of the system, it follows that the tilting angle with respect to the magnetic field axis is as small as $\Theta \leq 1 \times 10^{-3}$. For the trap parameters (see Table 2) used in the ISOLTRAP experiment Eq. (10) gives a maximum frequency shift $\Delta\nu^{\text{tilt}} = \Delta\omega^{\text{tilt}}/(2\pi) < 2$ mHz. This results in a maximum calibration error of less than 2×10^{-9} even for mass number differences up to $\Delta A = 100$. A final shimming of the superconducting magnet was performed after the tube was aligned in order to correct for additional inhomogeneities introduced by the tube itself.

3.3.1. Ion transfer section

The purpose of this section is to accept the beam delivered by the ion buncher and cooler and to transport it to the precision trap. The ion optical system (Fig. 12) consists of a number of adjustable slits (D4–D7) activated with INCHWORM (Burleigh Instruments) motors [68], an einzel lens (L4), two sets of deflectors (S3,S4) placed in the low field region of the magnet and a set of retardation electrodes (L5) in front of the trap. A microchannel-plate detector (MCP 2) helps to control the ion beam adjustment.

The lowest set of slits (D4) defines the entrance of the spectrometer part. A first set of steerers (S3) corrects the angle of the incoming beam which is then focussed by the einzel lens (L4) so as to properly enter the magnetic field. The second set of steerers (S4) is used for fine adjustment of the injection angle.

The injection of the ions has to be performed with a minimum pickup of transverse energy when the ions enter the increasing field of the superconducting magnet. This is necessary, since the resonance detection scheme used in ISOLTRAP is based on the detection of a change of the radial energy of the ion motion as discussed in Section 2.3. Such an injection of ions into the magnetic field is illustrated in Fig. 13 by calculated ion trajectories for three different injection conditions. The plotted lines represent the distances of the ion trajectories from the magnetic field axis. The dotted line shows a magnetic field line for comparison. Case (a) shows a good injection of ions into the magnetic field. The ions are focussed to a point about 20 cm below the center of the field. Practically no radial energy is picked up as the ions pass into the high field region. In case (b) the axis of the incoming beam is shifted by 2.2 mm parallel to the magnetic field axis. A large increase in radial energy is observed and, furthermore, a common maximum distance from the magnetic field axis at position z^*. Case (c) shows the injection of ions with the same displacement but with an injection angle such that the focus is again on the magnetic field axis. The energy pickup is considerably reduced and at

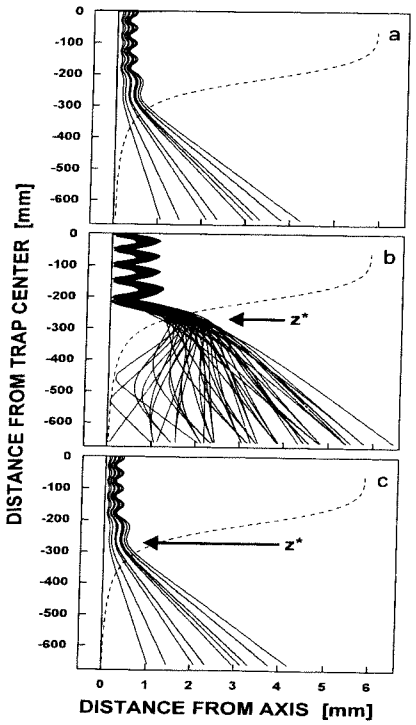

Fig. 13. The injection of a beam of ions of mass $A = 100$ into the magnetic field of the mass spectrometer part of ISOLTRAP. Plotted is the distance of the ion trajectories from the magnetic field axis. The horizontal scale is expanded. Case (a) shows a good injection of ions into the magnetic field. In case (b) the axis of the incoming beam is shifted by 2.2 mm parallel to the magnetic field axis. Case (c) shows the injection of ions with the same displacement but with an injection angle such that the focus is again on the magnetic field axis. Position z^* shows the optimal position for a diaphragm for the control of injection conditions that result in a minimum pickup of radial energy.

position z^* a minimum distance of the ion trajectories from the field axis is now observed. Placing a diaphragm at this position therefore allows the injection of the ions to be controlled since only for the correct focus and injection angle is good transmission achieved. The optimum position of the diaphragm is mass dependent. Therefore, two adjustable diaphragms have been installed, one for light (D6) and one for heavy ions (D7).

3.3.2. *The precision trap*

The trap has been designed for minimum magnetic and electric field imperfections over a large a volume as possible. This is essential for the ISOLTRAP experiments since, in the process used for observing the ion cyclotron resonance, the ion cannot be confined to a very small volume near the trap center. The choice of design was a highly compensated hyperbolic trap which offers the best compromise between a perfect field and a desirable trap size. Fig. 14 shows a cross-sectional view of the precision trap and Table 2 summarizes its dimensions and important parameters.

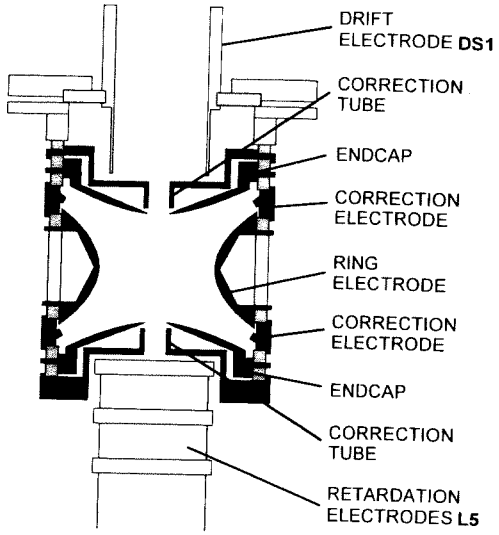

Fig. 14. Cross-sectional view of the high-precision trap TRAP 2 in the ISOLTRAP spectrometer. In addition, the retardation electrodes L5 and the first drift tube D1 are shown.

To allow incoming ions to be captured off-axis, the whole trap can be displaced parallel to the magnetic field axis by means of an INCHWORM motor. This results in the magnetron motion required for the cyclotron resonance detection as discussed in Section 2.3.

Deviations from the ideal quadrupole field are compensated by correction electrodes installed between the endcap and the ring electrode and at the holes in the endcaps re-

Table 2
Dimensions and important parameters of the precision trap (TRAP 2) in the mass spectrometer part

Trap characteristics	Highly compensated trap for the cyclotron frequency determinations with two sets of correction electrodes		
Trap materials	Oxygen-free high conductive (OFHC) copper, glass ceramics MACOR		
Vacuum	p	$< 10^{-8}$ mbar	
Trap dimensions	ρ_0	13.00 mm	
	z_0	11.18 mm	
	d	10.23 mm	
Magnetic field	B	6.0 T	
Potentials of trapping electrodes	Ring electrode	1.0 V	
	Endcaps	9.5 V	
Potentials of correction electrodes		Exp.	Calc.
	Correction ring	5.0 V	4.4 V
	Correction tube	12.2 V	11.9 V
Eigenfrequencies of an ion with mass number $A = 100$	ν_+	918 kHz	
	ν_-	1 kHz	
	ν_z	44 kHz	

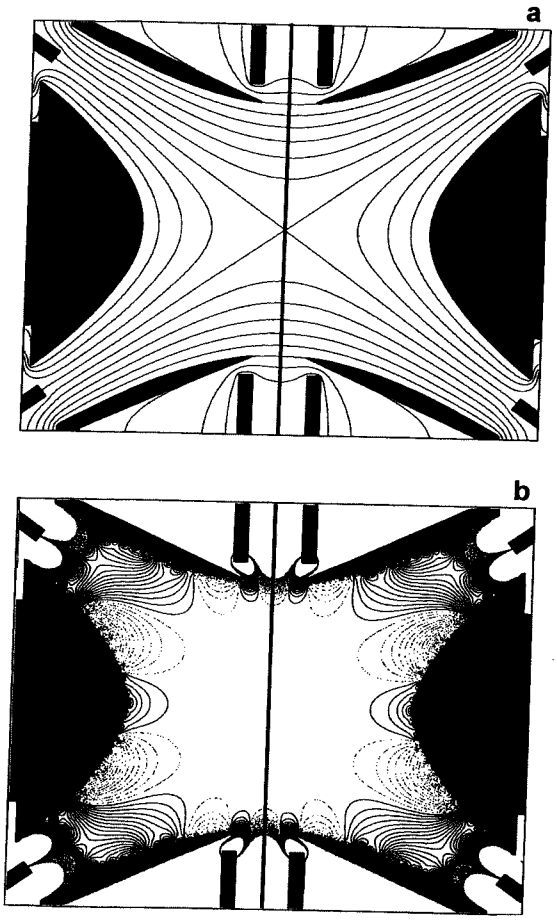

Fig. 15. (a) Equipotential lines for the compensated trap shown in Fig. 14. The distance between two lines is $0.1U_0$. (b) Residual electric potential ΔU after the subtraction of a pure quadrupole field. The distance between two equipotential lines is $10^{-4}U_0$. Only equipotential lines in the range $-49.5 \times 10^{-4} \leq \Delta U/U_0 \leq 49.5 \times 10^{-4}$ are shown. Dotted lines correspond to negative values.

quired for injection and ejection of ions [33,69]. Fig. 15a shows the equipotential lines that result from calculation of the electric field inside the precision trap. These calculations have been performed with an optimized relaxation method which was found to give the necessary accuracy, followed by a least-square fit to a pure quadrupole field to obtain the best settings for the correction electrodes [70]. Fig. 15b shows the deviation of the resultant field from that of a pure quadrupole, i.e. the sum of all higher multipoles. The distance between the equipotential lines in Fig. 15b corresponds to a potential change of $10^{-4}U_0$ where U_0 is the trapping potential. Expressed as multipoles the octupole coefficient is found to be $|C_4| \approx 10^{-5}$.

The calculations give directly the best theoretical settings for the correction electrodes. Based on a trapping voltage $U_0 = 8.5$ V these settings are listed in Table 2 together with those values determined experimentally (see Section 4.3). The values are in reasonable agreement within the numerical accuracy of the calculation and the mechanical tolerances of the trap.

The ring electrode of the trap is split into four segments for the creation of the azimuthal quadrupole RF field needed for the excitation of the ion motion at $\omega_c = \omega_+ + \omega_-$. In order to preserve the good quality of the electric trapping field the slits are only 0.2 mm wide.

Magnetic field inhomogeneities from the trap itself are kept small by use of materials with low susceptibility. The trap is constructed from OFHC copper and is gold plated. Glass ceramics (MACOR) are used for insulation. At room temperature MACOR has a susceptibility which is comparable to the value for copper. In addition, all parts are machined as thin as possible to minimize the magnetic-field distortions. Fig. 16 shows the calculated contributions to magnetic-field distortions of all electrodes and insulators of the precision trap shown in Fig. 14. In the region $-0.5z_0 < z < +0.5z_0$ the quadratic term of the relative magnetic field inhomogeneity has been determined to be as low as $|\Delta B/B| = 4 \times 10^{-7}(z/z_0)^2$. This means that for axial amplitudes ρ_z not exceeding 25% of the distance $2z_0$ between both endcaps a relative frequency shift in ω_c of less than 10^{-7} can be expected.

3.3.3. The drift section for time-of-flight detection

As discussed in Section 2.3 a time-of-flight technique is used for the detection of the gain of radial energy of the ions after the excitation of their motion in the trap. The drift section was designed to fulfill two demands: a maximum conversion of the gained radial energy into axial energy has to be achieved and the ions have to be transported to the detector which is placed outside the superconducting magnet 1.3 m from the trap. Therefore, the drift section (Fig. 12) can be divided into two functional parts. The first part provides the potentials for the energy conversion, the second part transports the ions to the detector without losses. Fig. 17 shows the electric potential and the magnetic field strength along the magnetic field axis in the sections close to the trap. Ions ejected from the trap are first brought out of the homogeneous region of the magnetic field with an energy of a few eV (DS1, see Fig. 12). At the beginning of the inhomogeneous part of the magnetic field the ions are retarded to the lowest possible energy without loss. They then drift through the region of high magnetic field gradient (DS2,DS3), where the radial energy of up to typically 10 eV that they have gained from the cyclotron resonance is converted into the same amount of axial energy. The following section of the drift tube has to transport the ions to the detector without losses. Because of the variation in the initial energy, the beam size at this point (typically 5 mm diameter) and the diverging magnetic-field lines, a two-stage acceleration (DS4,DS5) and an additional lens (DS7) are needed to focus all ions onto the detector (MCP 3).

The detector chamber is placed outside the magnet and

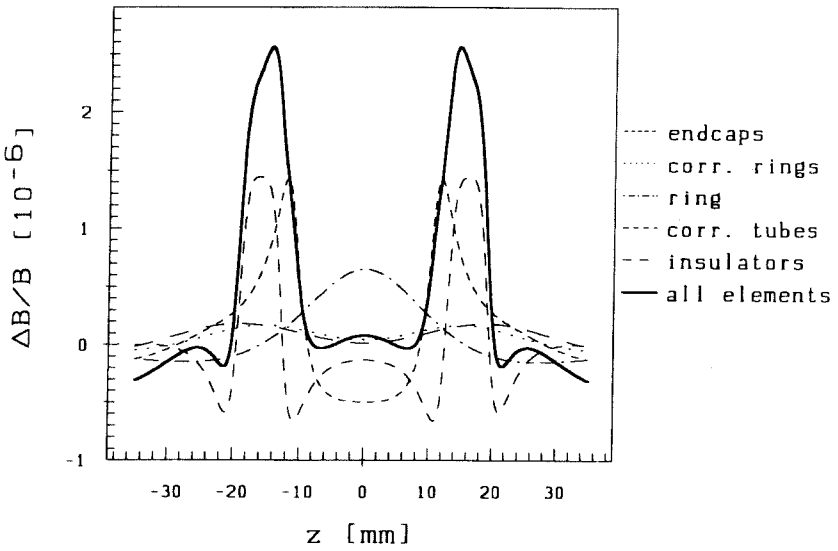

Fig. 16. Magnetic field inhomogeneity along the axis of the high-precision trap (Fig. 14). The contributions of the different electrodes and insulating parts of the precision trap to the total inhomogeneity (solid line) are shown.

can be disconnected from the trap region by means of an electro-pneumatic valve. This allows easy and fast replacement of the detector without the need to break the vacuum in the trap region. Furthermore, two detectors are provided which are mounted back to back on a rotational mechanical feedthrough. Each detector is a tandem microchannel-plate detector with an active diameter of 50 mm.

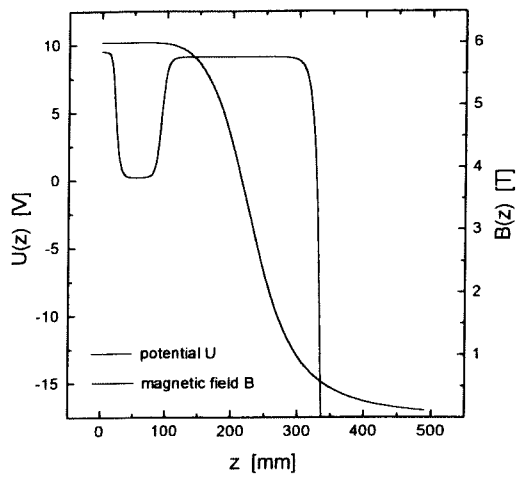

Fig. 17. Electric potential and magnetic field strength along the magnetic field axis in the first part of the drift section above the precision trap TRAP 2.

4. Experimental procedures

Several experimental procedures are applied in the ISOLTRAP mass measurements. The most important will be discussed, starting with the standard procedure for the determination of a cyclotron resonance, the determination of the mass of a certain isotope, the related calibration of the magnetic field, and optimization procedures for the parameters of the precision trap.

4.1. Cyclotron resonance measurement

A cyclotron resonance measurement starts with the collection of a sufficient number of ions from ISOLDE on the lower foil in the ion cooler and buncher. After turning the foil by 180° a number of steps are involved in the subsequent measurement cycle, as shown in Fig. 18. The foil facing the inside of the trap is current heated for 500 ms (1). The current is regulated to release a constant number of ions by surface ionization. A fraction of these ions loses enough energy by buffer gas collisions when passing through the trap to be captured. In order to avoid charge exchange, helium is normally used as buffer gas at a measured pressure of $p \approx 10^{-4}$ mbar. At the same time that the heating is started an RF voltage at the frequency ω_c of the ions to be centered is applied between the two pairs of opposite segments of the ring electrode (2). The excitation time is T_{RF} = 900 ms and the amplitude of the RF voltage typically V_{RF} = 0.3 V. The cooled and centered ion cloud is then ejected from the trap by simultaneously pulsing the potential of the lower endcap to U_{endcap} = 4 V and the potential of the ring electrode to U_{ring} = 2 V (3). The approximately homogeneous electric

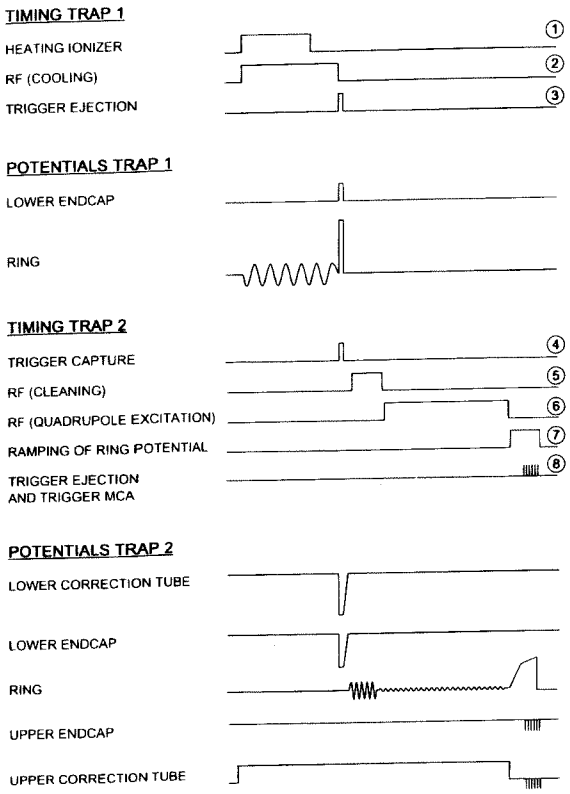

Fig. 18. Timing sequence of one measurement cycle as needed for a cyclotron resonance determination. The electrode potentials shown are those that are varied during the cycle (see text).

field of $E = 1.4$ V/cm ejects the ions from the trap.

The additional electrodes (L1) incorporated in the upper endcap accelerate the ions to an energy of 1 keV for transfer to the mass spectrometer. For their capture [71] the ions are retarded in front of the precision trap to an energy of a few eV. At the time of ejection of the ions from the ion buncher and cooler, the potentials of the lower endcap and the correction ring of the precision trap are lowered to $U_{low} = -2$ V (4). When the ion bunch has entered the trap the potentials of both electrodes are brought back to their normal operation voltages (see Table 2) within a few μs. The time interval T_{capt} between ejection of the ions with mass number A is $T_{capt} \approx 6\ \mu s \cdot \sqrt{A}$.

A preliminary excitation step (5) is used to remove unwanted ions which are still present due to the limited resolving power of the mass selective cooling process in the ion cooler and buncher. The cyclotron motion of the ions to be removed is strongly driven by an azimuthal dipole field. The field is created by connecting two neighbouring ring segments and applying the RF voltage between the two half rings. In order to eliminate more than one species during the excitation time of typically $T_{clean} = 250$ ms the different cyclotron frequencies are subsequently applied within this period. If a higher resolving power in the cleaning process is needed the ion motion is driven at $2\omega_+$ by means of an azimuthal quadrupole field set up with all four segments of the ring electrode. The higher resolving power is achieved because the line width is only determined by the excitation time.

For the cyclotron frequency determination the initially pure magnetron motion of the stored ions, obtained via the off-axis injection into the trap, has to be transformed into pure cyclotron motion as discussed in Section 2.3. In order to achieve this the ion motion is driven with an azimuthal quadrupole field with a frequency ν_{RF} close to the cyclotron frequency ν_c of the trapped ions (6). Typically, an excitation time $T_{RF} = 900$ ms is used, the amplitude of the RF voltage being of the order of $V_{RF} \approx 5$ mV.

Finally, the ions are ejected from the precision trap for the time-of-flight detection of the gained radial energy. The ejection is performed by slowly lowering the trapping potential (7) (i.e. raising the ring potential) while applying short negative pulses to the upper endcap and the correction ring (8), which has previously been set to the potential of the endcap. The use of several pulses allows the ions to be extracted as ion bunches with low axial energy spread. The ejection pulses are separated by a time interval which is roughly equal to the time of flight of the ion bunches to the detector.

Each of the ejected ion bunches arriving at the microchannel-plate detector is detected separately and the time resolved signal is summed in a multichannel analyser. Fig. 19 shows the time-of-flight distribution of ^{85}Rb ions for $\nu_{RF} \neq \nu_c$ and $\nu_{RF} = \nu_c$. In the latter case the mean time of flight is reduced by typically 30%.

A cyclotron resonance curve is obtained by repeating the measurement cycle (steps (1)–(8)) for different excitation frequencies ν_{RF} and plotting the average time of flight from the trap to the detector as a function of ν_{RF}. A typical resonance curve is shown in Fig. 20 for the case of ^{118}Cs, an unstable isotope with a half-life of $T_{1/2} = 17$ s.

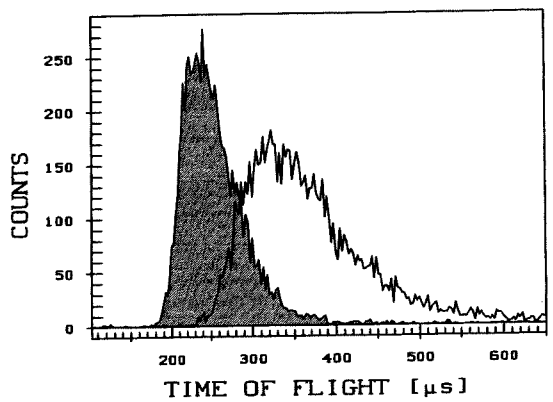

Fig. 19. Time-of-flight distribution of ^{85}Rb ions ejected from the precision trap and detected by MCP 3 for $\nu_{RF} \neq \nu_c$ (white) and $\nu_{RF} = \nu_c$ (grey).

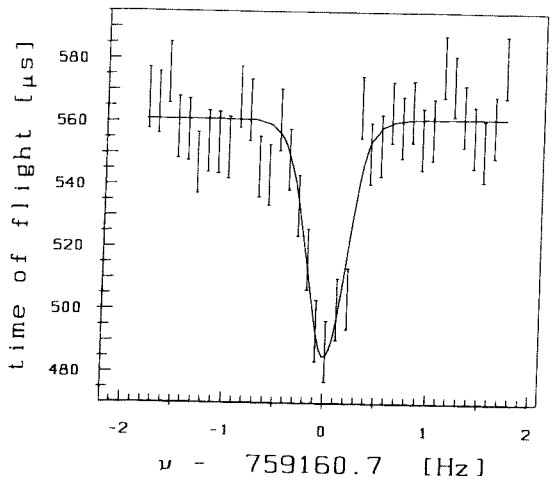

Fig. 20. Cyclotron resonance curve of unstable ^{118}Cs ions as obtained from the mean time of flight as a function of the applied frequency ν_{RF}.

4.2. Calibration of the magnetic field

The magnetic field B has to be known for a mass determination via the cyclotron frequency $\omega_c = (q/m)B$. It can be determined by measurement of the cyclotron frequency of a reference ion with well known mass. The mass m of the ion of interest is then given by the ratio of the cyclotron frequencies $m = m_{ref} \cdot \nu_{ref}/\nu$ and the mass m_{ref} of the reference ion.

As discussed in Section 2.2.3 one source of systematic errors can be the stability of the magnetic field. Fig. 21 shows a typical reference measurement over a time period of 140 h.

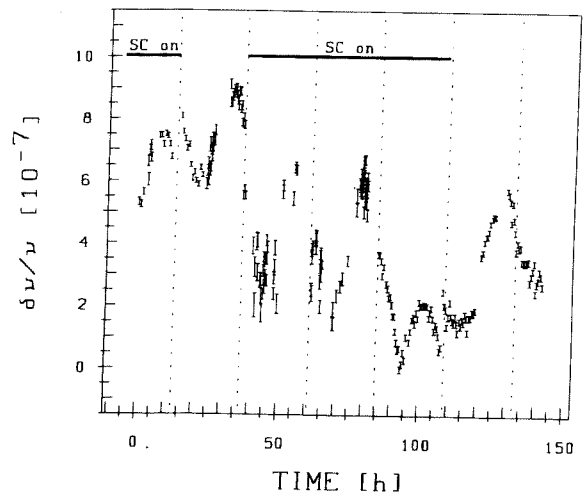

Fig. 21. Time variation of the magnetic field as shown by the cyclotron frequency for ^{133}Cs ions over a period of 140 h. The horizontal lines in the upper part of the figure mark those periods in which the synchrocyclotron 30 m away from the trap was switched on. The dashed vertical lines mark the beginning of a new day.

The magnetic field shows an oscillation with a period of 24 h. This behaviour was found to be due to the temperature dependence of the susceptibility of the vacuum tube containing the precision trap and the day–night temperature variations in the experimental hall at ISOLDE-2. Furthermore, the operation of the magnet of the CERN synchrocyclotron at a distance of about 30 m from the ISOLTRAP spectrometer has a significant effect on the magnetic field.

From the figure it is evident that a magnetic field calibration via a reference measurement should be performed at intervals short enough to resolve the changes of the magnetic field in time. In the on-line runs performed so far with ISOLTRAP, stable ^{85}Rb and ^{133}Cs have mainly been used as reference isotopes. Before and after each run a longer series of cyclotron frequency measurements of these isotopes has normally been performed in order to check the magnetic-field stability and the general performance of the spectrometer. During the on-line measurements on radioactive isotopes reference measurements have been carried out at regular intervals of several hours.

4.3. Tuning of trap parameters

In order to achieve high accuracy it is important to find the best settings for the correction electrodes of the precision trap. Two different approaches are used: in the first procedure the amplitude of the RF voltage for the ν_c excitation of the ions is chosen to be higher than needed for a full conversion of magnetron into cyclotron motion. This results in a reduction of the central peak of the resonance and an increase of the side peaks. If there are imperfections in the electrostatic trapping field the resonance curve will show asymmetry (see Section 2.3 and Ref. [33]). The tuning is therefore performed by changing the settings of the correction electrodes until a completely symmetric curve is obtained. The second procedure uses ν_+ resonances obtained by dipole excitation of the ion motion. These resonances are much more sensitive to electric field imperfections because frequency shifts do not cancel as in the case of quadrupole excitation. One criterion is to achieve the smallest possible linewidth together with a maximum time-of-flight effect in resonance. The other is to observe no frequency shift if the excitation amplitude is varied, which corresponds to a variation of the average amplitude of the cyclotron motion. Both procedures give consistent results for the settings, which are listed in Table 2 together with calculated values.

Intentionally wrong settings for the correction electrodes are useful for the determination of the correct timing for the ion capture in the precision trap. As discussed in Section 4.1 the potentials of the lower correction electrode and endcap are raised again to their normal operation voltage at time T_{capt} after the ejection of the ions from the lower trap. The aim is to capture the ions with a minimum pickup of axial energy. A slightly too early or too late closing of the trap will cause the whole ion cloud to perform an axial oscillation and to probe the deliberately created field

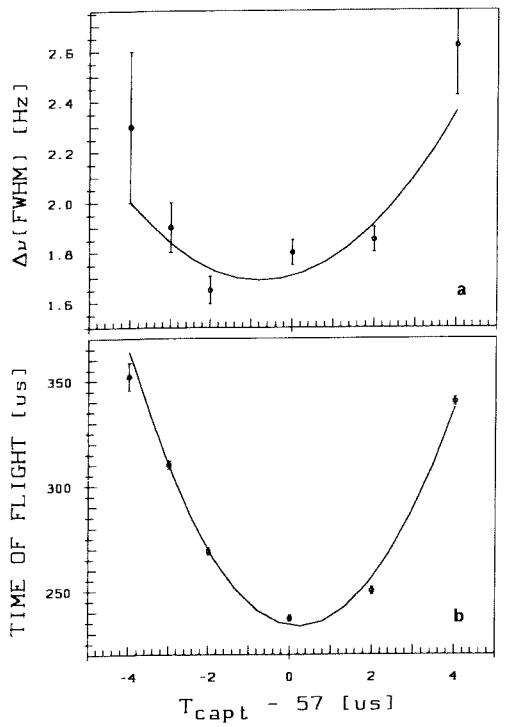

Fig. 22. Determination of the correct timing for ion capture in the precision trap by means of ν_+ resonances and intentionally created electric field imperfections. (a) The linewidth $\Delta\nu$(FWHM) of the resonances; (b) the time of flight in resonance as a function of the capture time T_{capt}.

imperfections. This can be seen directly in the resonance curves. Fig. 22 shows the linewidth of ν_+ resonances (a) and the time of flight in resonance (b) both as functions of the capture time T_{capt} for the case of ^{85}Rb ions. The optimum capture time is $T_{capt} = 57$ μs. For the example shown here, the timing for other isotopes can be determined from $T_{capt}(X)/T_{capt}(^{85}\mathrm{Rb}) = \sqrt{M(^{85}\mathrm{Rb})/M(X)}$.

We conclude this section by discussing the determination of the required excitation amplitude V_{RF} for the quadrupole excitation at ν_c. First, the cyclotron frequency ν_c of the ion species under investigation is determined. Then the excitation frequency ν_{RF} is set to $\nu_{RF} = \nu_c$ and the time of flight of the ions is measured as a function of the excitation amplitude V. Fig. 23 shows such a measurement. The curve directly reflects the periodic conversion of magnetron into cyclotron motion and vice versa. The minimum on the far left corresponds to a single magnetron–cyclotron conversion, the following maximum to a magnetron–cyclotron–magnetron conversion and in the second minimum two magnetron–cyclotron conversions have occurred. The proper excitation amplitude V_{RF} for a single conversion is most precisely determined from one of the maxima in the time of flight which appear at excitation amplitudes $V_n = 2nV_{RF}$. From Eq. (14) it follows that the product of excitation time and amplitude $T_{RF} \cdot V_{RF}$ is constant and to first order mass independent. A

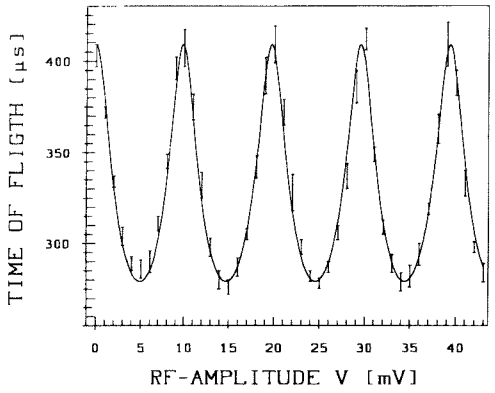

Fig. 23. Mean time of flight of the ions as a function of the applied RF amplitude V of the azimuthal quadrupole field with frequency $\nu_{RF} = \nu_c$. The solid line shows a fit of the theoretically expected function to the data.

typical value for this product is $T_{RF} \cdot V_{RF} = 4.9 \times 10^{-3}$ V s. Variations of this value arise from the frequency dependence of the voltages actually arriving at the trap electrodes. Therefore, the determination of $T_{RF} \cdot V_{RF}$ has to be carried out for each mass region to be investigated.

5. Experimental control and data acquisition

The control of the experiment and the on-line evaluation is performed by a LSI 11/73 (Digital Equipment Corporation) based computer system. The link to the experiment is achieved via CAMAC. The complex timing needed in the ISOLTRAP experiment (see Fig. 18) is controlled by two home-built 12-channel timing memories with a time resolution of 1 μs. All pulse generators required for ejection and capture of ions, a number of relays for the heating and the output of the frequency synthesizers are triggered or gated by these programmable memories.

For the quadrupole excitation of the ion motion at ν_c a high-precision frequency generator (Schomandl MS100) with a frequency stability of $< 10^{-9}$ per hour and a minimum step size of 0.1 Hz is used. Additional frequency synthesizers (Hewlett Packard HP3325) serve for the cleaning of unwanted ion species in the precision trap and for the mass selective cooling process in the lower trap.

The time-of-flight distribution of the ions is measured by a home-built multi-channel analyser with a maximum input count rate of 100 MHz and dwell times between 20 ns and 2.56 μs. This device can be retriggered and directly sums the time-of-flight spectra of the sequence of ion bunches ejected from the precision trap.

For every cycle the data are read into the computer and made available to the on-line data evaluation after each scan over the excitation frequencies. The number of events detected in each cycle is used to regulate the current supply for the heating of the foil in the ion cooler and buncher via

a CAMAC-DAC. This allows the average count rate to be kept constant until all the collected atoms are used up.

The on-line data evaluation software allows the calculation of the resonance curves from the measured time-of-flight spectra, the fitting of these curves, the analysis of the fit results and a first calculation of mass values. Such a nearly complete evaluation of the data is indispensable for on-line measurements, where only limited time is available and problems and faults have to be detected immediately.

The final evaluation of the data is performed on a VAX system. It differs from the on-line evaluation in that the measured time dependence of the magnetic field is properly included in the calculation of the frequency ratios. A more detailed description of the final data evaluation can be found in Refs. [72,78].

6. Performance

Table 3 summarizes the isotopes investigated so far with the ISOLTRAP spectrometer [31,43,72–78]. The stable isotopes ^{39}K, ^{85,87}Rb and ^{133}Cs listed in the table were used for the magnetic-field calibration. The high performance of the Penning trap mass spectrometer allowed the determination of the mass values of all isotopes with accuracies of $\delta m/m \approx 10^{-7}$ (see Section 6.2). New mass values could be determined in the cases of ^{78,79}Sr, ^{122m}Cs, ^{124,126}Ba and ^{230}Ra [72,75,78]. The shortest-lived isotope investigated so far is ^{142}Cs with a half-life of $T_{1/2} = 1.8$ s.

In the following those properties of the ion cooler and buncher and the mass spectrometer part which are essential for high-accuracy mass determination of unstable isotopes will be discussed. These are the mass selectivity and the cooling limit of the buffer gas cooling technique, the line shape and resolving power obtained in the precision trap, the achievable accuracy, and the efficiency and applicability of ISOLTRAP.

6.1. Ion cooling and bunching

In order to reach a high accuracy one important measure is the minimization of the motional amplitudes of trapped ions by cooling. In the case of ISOLTRAP the cooling is performed in the ion cooler and buncher described in Section 3.2. With the applied buffer gas cooling technique (Section 2.4) it is expected that the final temperature of the ion cloud will be approximately that of the buffer gas. Fig. 24 shows the result of a measurement where cooled ^{133}Cs ions were ejected from the trap and their energy analysed by a retardation technique [64]. The figure shows the number of Cs ions detected by MCP 1 as a function of the repelling voltage applied in front of the detector. The observed spectrum agrees with the spectrum (full line) calculated for an ion temperature of 300 K. For comparison, the dotted line corresponds to a temperature of 1000 K.

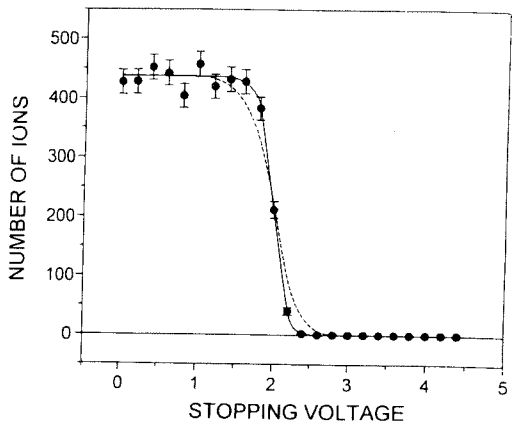

Fig. 24. Number of Cs ions detected as a function of the repelling voltage applied in front of detector MCP 1. The observed distribution is in agreement with the calculated distribution (solid line) for ions with a temperature of 300 K in the trap. For comparison, the dotted line corresponds to a temperature of 1000 K.

To achieve high accuracy it is also important to store only one ion species at any one time in the precision trap,

Table 3
Isotopes for which cyclotron resonances have been determined with ISOLTRAP

Element	Mass number
K	39
Rb	75–89, 90m, 91–94
Sr	78–83, 91–95
Cs	117–121, 122+122m, 122m, 123–140, 142
Ba	124, 126, 128, 138–144
Fr	209–212, 221, 222
Ra	226, 230

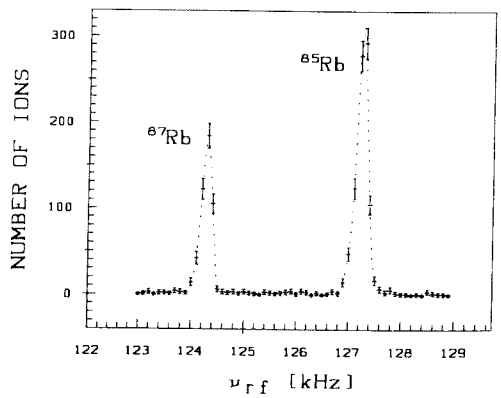

Fig. 25. Number of Rb ions ejected from the buncher and cooler trap and detected with MCP 1 as a function of the applied frequency. The resonance for ^{85}Rb and ^{87}Rb has been obtained with a helium pressure of $p_{He} = 2 \times 10^{-4}$ mbar.

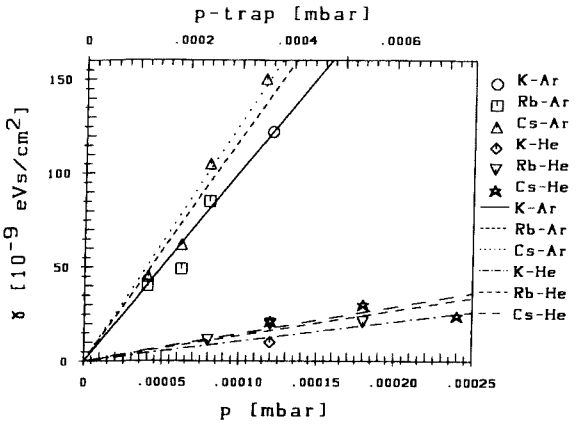

Fig. 26. Friction coefficient γ for various ions as a function of the applied gas pressure of helium and argon. The friction coefficients are calculated from the measured time constant α_- of the increase of the magnetron motion (symbols). The straight lines result from ion mobility data if a pressure p_{trap} three times higher than the measured values p is assumed.

as discussed in Section 2.2.4. The mass selectivity of the cooling process allows a first purification of the ion ensembles delivered by ISOLDE. The mass selectivity that can be achieved for stable Rb ions is illustrated in Fig. 25. It shows the cooling resonance as obtained from the number of ions ejected from the cooler and buncher trap and detected by MCP 1 as a function of the applied RF frequency ν_{cool}. The resonance curves have a linewidth of $\Delta\nu_{cool}$(FWHM) $\approx$ 255 Hz corresponding to a mass resolving power of 500. The best resolving powers have been obtained at a pressure of $p = 2 \times 10^{-4}$ mbar and an RF amplitude of $V_{cool} = 0.3$ V. The limit of the resolving power is mainly determined by the inhomogeneity of the magnetic field and electric field imperfections in the trap. Nevertheless, it is sufficient for the complete removal of isotopic contamination present in the ISOLDE ion beam.

The simple theory of a damping force acting on the ion motion has been found to be a good description for the cooling by buffer gas. The increase of the magnetron motion can be directly observed by first centering the ions and then measuring the number of ejected ions as a function of the time delay between switching off the RF field and the ion ejection. From the number of ions as a function of the time delay one can directly extract the time constant α_- and via Eq. (21) the friction coefficient γ. Fig. 26 shows γ as a function of the pressure for helium and argon as buffer gas and for different ion species. One observes a linear dependence from the measured gas pressure p, a large difference for the two gases and a small element dependence. This is in good agreement with the calculated behaviour (straight lines) based on the published ion mobility values for potassium, rubidium and cesium ions in these gases [79,80]. From the known ion mobilities the pressure p_{trap} in the trap is found to be three times higher than determined by the Penning gauge at a distance of about 50 cm from the trap.

6.2. Precision and accuracy

Accurate knowledge of the line shape of the cyclotron resonance curve is important for detecting residual trap imperfections which limit the achievable accuracy. Only if the line shape is known and symmetric can the value of the cyclotron frequency be determined from the center of the curve. Fig. 27 shows a cyclotron resonance curve of ^{133}Cs obtained with high statistics. The line shape agrees perfectly with the fit of the theoretical profile (solid line) discussed in Section 2.3. Only six fit parameters were needed to achieve this: the center of the resonance, the maximum gained radial energy, the initial axial energy, and three parameters describing the transformation of radial energy into time of flight.

The measurement was performed with an excitation time T_{RF} = 900 ms. The minimum linewidth expected from Eq. (18) is $\Delta\nu_c$(FWHM) = 0.9 Hz. Due to the non-linear conversion of radial energy into time of flight as discussed in Section 2.3 a larger linewidth of $\Delta\nu_c$(FWHM) = 1.1 Hz is observed which corresponds to a resolving power of $R = \nu_c/\Delta\nu$(FWHM) $\approx 0.6 \times 10^6$. The highest resolving power observed with the discussed version of the ISOLTRAP spectrometer is $R = 2 \times 10^6$ in the case of 3 s excitation of ^{85}Rb ions.

The statistical accuracy $\delta\nu$ (or precision) with which the center of a single resonance can be determined is typically 10% of the linewidth for a resonance curve with about 1000 ions detected. For an ion with mass number A = 100 this corresponds to $\delta\nu/\nu \approx 10^{-7}$.

The reproducibility of the data is illustrated in Fig. 28. The figure shows the histogram of the mass excess values obtained from 34 measured frequency ratios for the case of ^{77}Rb with ^{85}Rb as the reference isotope. The measurements have been performed in two separate runs. The data follow a normal distribution and the standard deviation of the fitted Gaussian is σ = 6.7 keV corresponding to a relative deviation of $\sigma/m = 9 \times 10^{-8}$. In the case shown here the

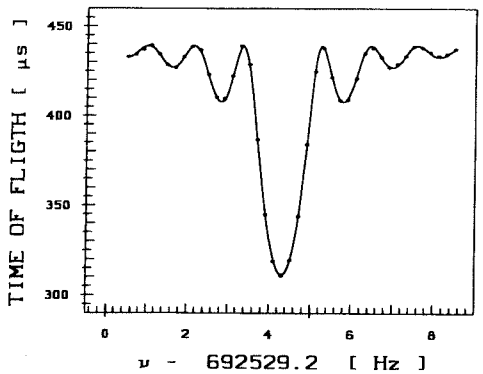

Fig. 27. Cyclotron resonance for ^{133}Cs ions obtained from the mean time of flight as a function of the frequency of the azimuthal quadrupole field. The solid curve shows a fit with the theoretically expected line shape.

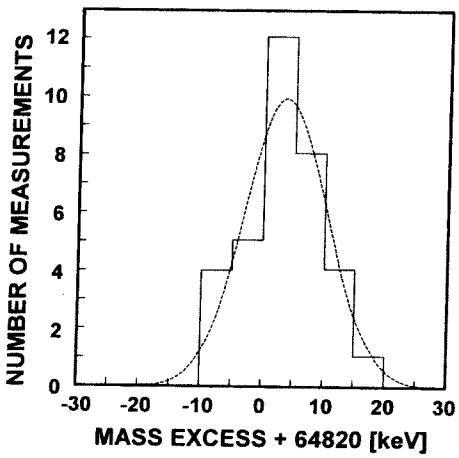

Fig. 28. Histogram of the results of a sequence of 34 mass determinations for ^{77}Rb. The data follow a normal distribution and the standard deviation of the fitted Gaussian is σ = 6.7 keV.

mean value can be determined with an accuracy of about 1.5×10^{-8}, which is a typical figure for the statistical accuracy obtained in our measurements on unstable isotopes.

As discussed in Section 2.2 there are a number of sources of frequency shifts that lead to systematic errors in the mass determination. Mass dependent systematic errors (Eq. (9)) can be checked via the determination of frequency ratios of ions very different in mass. Such checks have frequently been performed with the ISOLTRAP spectrometer with ^{85}Rb, ^{87}Rb and ^{133}Cs ions. With ^{85}Rb as reference isotope the mass value of the nearby ^{87}Rb is in agreement with the literature value [1] within the uncertainty $\Delta m/m = 3 \times 10^{-8}$ of this value. In the case of ^{133}Cs, which corresponds to a mass number difference of $\Delta A = 48$, agreement is achieved within typically $\Delta m/m < 10^{-7}$. This means that for smaller mass differences such as those in an isotopic chain, the possible mass dependent systematic error is well below 10^{-7}.

Magnetic field changes can be an important source of systematic errors in on-line runs. Due to the limited beam time available one has to find a compromise between the number of reference measurements (see Section 4.2), which determines the uncertainty of the magnetic field as a function of time, and the number of cyclotron frequency measurements on unstable isotopes. Normally, the magnetic field calibration can be performed with an uncertainty of $\delta B/B \approx 10^{-8}$. Nevertheless, unexpected jumps of the magnetic field of up to $\Delta B/B \approx 10^{-7}$ have occasionally been observed.

The effect of ion–ion interactions discussed in Section 2.2.4 is avoided by carefully removing all unwanted ions. The mass selective buffer gas cooling applied in the ion cooler and buncher removes isotopic contamination. Contaminating ions still present in the precision trap are either isobars or isomers. In the case of isobars these can be removed by strongly driving their cyclotron motion. With the $2\nu_+$ excitation it was possible to remove isobars with a

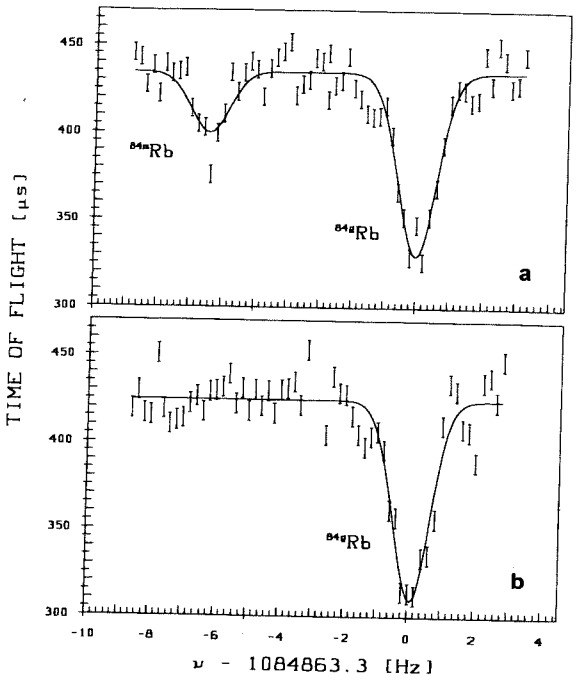

Fig. 29. Cyclotron resonances for ^{84}Rb ions. The measurements were performed (a) shortly after the collection of the ions and (b) with a delay of several half-lives of the isomeric state.

relative mass difference of $\Delta m/m \geq 10^{-5}$, which is sufficient for most cases. In the case of isomers or isobars with a small relative mass difference of $\Delta m/m < 10^{-5}$ one can make use of the generally different nuclear half-lives of the two ion species and let the shorter-lived contamination decay on the collection foil before starting the measurement. In the case of isotopes with comparable half-lives this technique cannot be applied. Here, the procedure is to determine the frequency shift as a function of the number of detected ions and to perform the mass measurement with a small ion number for which the resulting shifts are negligible within the desired accuracy. A measurement where the latter procedure was successfully applied is shown in Fig. 29. The upper part shows the cyclotron resonance curve for ^{84}Rb with ions in the nuclear ground and isomeric state simultaneously trapped. Two resonances are observed, one for the ground-state nucleus and one for the isomer. This measurement was performed with an average of N = 15 detected ions per cycle. It was preceded by a series of measurements with higher count rates and various delays between the collection of the ISOLDE ions on the foil and the start of the measurement, which have been described in detail in Ref. [43]. For higher count rates considerable frequency shifts were observed. The lower part of the figure illustrates that the shift is negligible for the case when 15 ions were detected from each trap loading. It shows the cyclotron resonance of only the ground-state nuclei obtained by letting

the isomeric state decay before the start of the measurement. The mass difference between ground and isomeric state, $\Delta m = 464(7)$ keV, evaluated from the low count-rate measurements is in perfect agreement with the value of $\Delta m = 463.7(10)$ keV known from nuclear spectroscopy.

As discussed above, the statistical uncertainty in the mass determination is typically a few parts in 10^8 and in test measurements on stable isotopes a comparable accuracy has been achieved. For on-line measurements, where only limited time can be devoted to the calibration of the magnetic field and the checking of all experimental parameters, systematic errors might occur. In order to cover these in the final uncertainty of the mass values, a conservative estimate of 1×10^{-7} is added quadratically to the statistical errors of the final mass values [72,75,78].

6.3. Efficiency

Since the production rates for unstable isotopes of interest are usually low, a high efficiency of the spectrometer is needed. The total efficiency

$$\epsilon_{\mathrm{tot}} = \epsilon_{\mathrm{bunch}} \cdot \epsilon_{\mathrm{trans}} \cdot \epsilon_{\mathrm{capt2}} \cdot \epsilon_{\mathrm{MCP}} \qquad (22)$$

of the ISOLTRAP spectrometer is determined by a number of factors: the efficiency $\epsilon_{\mathrm{bunch}}$ of the collecting and bunching of the ISOLDE ions; the transfer efficiency $\epsilon_{\mathrm{trans}}$ from one trap to the other; the capture efficiency $\epsilon_{\mathrm{capt2}}$ in the precision trap (TRAP 2); and the detector efficiency ϵ_{MCP}. Only ϵ_{tot}, $\epsilon_{\mathrm{trans}}$ and $\epsilon_{\mathrm{capt2}}$ have been measured in the ISOLTRAP spectrometer. Assuming a reasonable value for the detector efficiency ϵ_{MCP} allows the indirect determination of the bunching efficiency $\epsilon_{\mathrm{bunch}}$.

The total efficiency $\epsilon_{\mathrm{tot}} = N_{\mathrm{MCP\,3}}/N_{\mathrm{foil}}$ is defined as the ratio of the total number $N_{\mathrm{MCP\,3}}$ of ions detected with MCP 3 and the number N_{foil} of ions collected on the foil. For alkali ions delivered by the test source with 1 keV energy the total efficiency has been determined to be $10^{-4} < \epsilon_{\mathrm{tot}} < 10^{-3}$.

The capture efficiency $\epsilon_{\mathrm{capt2}} = N_{\mathrm{capt2}}/N_{\mathrm{pass}}$ in the precision trap can be determined by comparing the number N_{capt2} of ions detected after capture and subsequent ejection to the number N_{pass} of ions passing through the trap if this is set to a potential lower than the energy of the ions. It is close to $\epsilon_{\mathrm{trap}} = 100\%$.

The transfer efficiency $\epsilon_{\mathrm{trans}} = N_{\mathrm{MCP\,1}}/N_{\mathrm{MCP\,3}}$ is defined as the number $N_{\mathrm{MCP\,1}}$ of ions detected with the lower detector MCP 1 to the number $N_{\mathrm{MCP\,3}}$ of ions observed with MCP 3. Assuming identical efficiencies for both detectors leads to $\epsilon_{\mathrm{trans}} = 100\%$.

Assuming a detector efficiency of $\epsilon_{\mathrm{MCP}} = 25\%$ and using Eq. (22) yields a value of typically $\epsilon_{\mathrm{bunch}} \approx 10^{-3}$ for the bunching efficiency for alkali ions from the test source. The bunching efficiency $\epsilon_{\mathrm{bunch}} = \epsilon_{\mathrm{rel}} \cdot \epsilon_{\mathrm{ion}} \cdot \epsilon_{\mathrm{capt1}}$ is a product of the efficiencies for the ion release from the foil ϵ_{rel}, the surface ionization ϵ_{ion}, and the capture in the cooler and buncher trap $\epsilon_{\mathrm{capt1}}$. For alkali and alkali earth elements the release efficiency from a rhenium foil at a temperature of $T > 1700$ K is practically $\epsilon_{\mathrm{rel}} = 100\%$. The ionization efficiency ϵ_{ion} is determined by Langmuir's equation and depends exponentially on the difference between the work function ϕ of the foil material and the ionization potential W_{i} of the element. In general, the ionization efficiency is high and nearly temperature independent if $\phi > W_{\mathrm{i}}$ and strongly temperature dependent if $\phi < W_{\mathrm{i}}$. For a rhenium foil with $\phi = 5.1$ eV $\epsilon_{\mathrm{ion}} = 100\%$ for all alkali elements. For the alkali earth elements and a foil at a temperature that exceeds $T = 2000$ K with ($\phi < W_{\mathrm{i}}$), the values of ϵ_{ion} are about 4% for strontium, 30% for barium and 20% for radium.

The capture efficiency $\epsilon_{\mathrm{capt1}}$ is determined by the energy loss of the ions due to buffer gas collisions during their flight through the trap and by the initial energy spread of these ions. From the data of the ion mobility in helium at a pressure of $p = 10^{-4}$ mbar, the axial frequency of an ion with mass number $A = 100$ and a typical potential drop of ≈ 1 V across the foil during the heating process, the maximum value of the efficiency is estimated to be $\epsilon_{\mathrm{trap}}^{\mathrm{max}} = 10^{-3}$. The efficiency of ion capture in the lower trap is therefore the limiting factor in the present total efficiency of ISOLTRAP.

6.4. Applicability

Presently, the ISOLTRAP spectrometer can only be applied to surface-ionizable elements. The elements that can be studied with ISOLTRAP at ISOLDE are shaded in the periodic table shown in Fig. 9. For the indicated cases the ionization efficiency is at least 2% for a rhenium foil temperature of 1700 K. Mass measurements on isotopes of the remaining elements require other techniques which are presently under investigation and development [31].

Not all isotopes of those elements marked in Fig. 9 can be investigated. The limiting factors are the half-life of the isotope $T_{1/2}$, its production rate Y, the overall efficiency ϵ_{tot} of the spectrometer for this element, and the total time T_{tot} for one measurement cycle (see Fig. 18). The minimum yield Y (ions per second) needed from the ISOLDE separator for a certain number N of detected ions per cycle is theoretically

$$Y = N \cdot T_{\mathrm{tot}}^{-1} \cdot \epsilon_{\mathrm{tot}}^{-1} \cdot 2^{T_{1/2}/T_{\mathrm{tot}}}. \qquad (23)$$

Fig. 30 shows the yield-times-efficiency product $Y \cdot \epsilon_{\mathrm{tot}}$ as a function of the half-life $T_{1/2}$. The curve (solid line) is calculated for $N = 1$ detected ions and assuming the lower limit of T_{tot} to be the half-life $T_{1/2}$ of the isotope. In addition, the figure shows the resolving power-times-mass number product $R \cdot A$ (dotted line) assuming that the excitation time in the precision trap $T_{\mathrm{RF}} \approx T_{\mathrm{tot}}$ dominates the total time for one cycle. If an ion with mass number $A = 100$ and half-life $T_{1/2} = 1$ s is to be investigated and if the spectrometer has an efficiency of $\epsilon_{\mathrm{tot}} = 10^{-5}$ for this element, then a minimum yield of $Y = 2 \times 10^5$ s^{-1} is needed and the resolving power can be as high as $R = 10^6$. For shorter-lived isotopes the required yield increases and the achievable resolving power decreases. Therefore, the main application of ISOLTRAP is

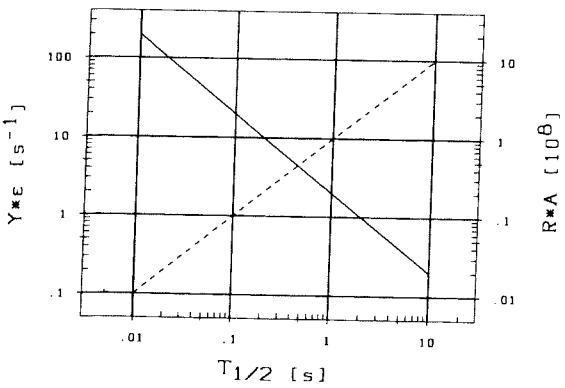

Fig. 30. Yield-times-efficiency product $Y \cdot \epsilon_{tot}$ as a function of the half-life $T_{1/2}$. The curve is calculated for $N = 1$ detected ions and a lower limit of the cycle time of $T_{tot} = T_{1/2}$. In addition, the resolving power-times-mass number product $R \cdot A$ for $T_{RF} \approx T_{tot}$ is given.

the investigation of light and heavy isotopes with half-lives of seconds and longer. Also, shorter-lived isotopes can be investigated, especially in the case of light masses for which the resolving power increases with decreasing mass number A and thus compensates for the shortening of the excitation time T_{RF}.

7. Conclusions

The tandem Penning trap mass spectrometer ISOLTRAP has been designed to meet the particular requirements of mass measurements on very small quantities of heavy and short-lived radioisotopes. It has proven to be a powerful instrument for the measurement of atomic masses. A large number of isotopes of alkali and alkali earth elements has already been investigated and accuracies in the mass determination of 0.1 ppm have been achieved. The high resolving power allowed the nuclear isomeric and ground states of an atom to be resolved for the first time by mass spectrometry. For many very unstable isotopes the accuracy of their mass values could be increased by one order of magnitude [31,72,75–78]. Wrong mass values could be tracked down in a number of cases and be assigned to wrong Q_β values. The measurements carried out not only improved the accuracy of the mass values of the investigated nuclei but also improved those of neighbouring isotopes of other elements due to the manifold links between them [76].

Presently, developments are going on in order to extend the applicability of the ISOLTRAP spectrometer to other elements, to increase its efficiency and to further improve the accuracy of the mass determination [31]. In the future, ISOLTRAP will become a spectrometer that can be applied to most of the isotopes available at ISOLDE. This will not only allow a more systematic investigation of the nuclear mass surface but will also allow study of cases of particular interest.

Acknowledgement

This work was funded by the German Federal Minister for Research and Technology (BMFT) under contract number 06 Mz-501-I and by NSERC of Canada. Travel support by NATO under grant number CRG 900675 is also acknowledged.

References

[1] G. Audi and A.H. Wapstra, Nucl. Phys. A 565 (1993) 1; G. Audi, A.H. Wapstra and M. Dedieu, Nucl. Phys. A 565 (1993) 193.
[2] C. Thibault, R. Klapisch, C. Rigaud, A.M. Poskanzer, R. Prieels, L. Lessard and W. Reisdorf, Phys. Rev. C 12 (1975) 644.
[3] M. Epherre, G. Audi, C. Thibault, R. Klapisch, G. Huber, F. Touchard and H. Wollnik, Phys. Rev. C 19 (1979) 1504.
[4] G. Audi, M. Epherre, C. Thibault, A. Wapstra and K. Bos, Nucl. Phys. A 378 (1982) 443.
[5] G. Audi, A. Coc, M. Epherre-Rey-Campagnolle, G. le Scornet, C. Thibault and F. Touchard, Nucl. Phys. A 449 (1986) 491.
[6] K.S. Sharma, E. Hagberg, G.R. Dyck, J.C. Hardy, V.T. Koslowsky, H. Schmeing, R.C. Barber, S. Yuan, W. Perry and M. Watson, Phys. Rev. C 44 (1991) 2439.
[7] D.J. Vieira, J.M. Wouters, K. Vaziri, R.H. Kraus, H. Wollnik, G.W. Butler, F.K. Wohn and A.H. Wapstra, Phys. Rev. Lett. 57 (1986) 3253.
[8] J.M. Wouters, D.J. Vieira, H. Wollnik, G.W. Butler, R.H. Kraus, Jr. and K. Vaziri, Nucl. Instr. and Meth. B 26 (1987) 286.
[9] J.M. Wouters, R.H. Kraus, D.J. Vieira, G.W. Butler and K.E.G. Löbner, Z. Phys. A 331 (1988) 229.
[10] X.L. Tu, X.G. Zhou, D.J. Vieira, J.M. Wouters, Z.Y. Zhou, H.L. Seifert and V.G. Lind, Z. Phys. A 337 (1990) 361.
[11] X.G. Zhou, X.L. Tu, J.M. Wouters, D.J. Vieira, K.E.G. Löbner, H.L. Seifert, Z.Y. Zhou and G.W. Butler, Phys. Lett. B 260 (1991) 285.
[12] H.L. Seifert, J.M. Wouters, D.J. Viera, H. Wollnik, X.G. Zhou, X.L. Tu, Z.Y. Zhou and G.W. Butler, Z. Phys. A 349 (1994) 25.
[13] A. Gillibert, L. Bianchi, A. Cunsolo, B. Fernandez, A. Foti, J. Gastebois, Ch. Gregoire, W. Mittig, A. Peghaire, Y. Schutz and C. Stephan, Phys. Lett. B 176 (1986) 317.
[14] A. Gillibert, W. Mittig, L. Bianchi, A. Cunsolo, B. Fernandez, A. Foti, J. Gastebois, Ch. Gregoire, Y. Schutz and C. Stephan, Phys. Lett. B 192 (1987) 39.
[15] N.A. Orr, W. Mittig, L.K. Fifield, M. Lewitowicz, E. Plagnol, Y. Schutz, Zhan When Long, L. Bianchi, A. Gillibert, A.V. Belozyorov, S.M. Lukynov, Yu.E. Penionzhkevich, A.C.C. Villari, A. Cunsolo, A. Foti, G. Audi, C. Stephan and L. Tussan-Got, Phys. Lett. B 258 (1991) 29.
[16] G. Auger, M. Bajard, D. Bibez, E. Baron, P. Bricault, A. Chabert, J. Ferme, K. Fifield, L. Gadart, A. Gillibert, A. Joubert, M. Lewitowitz, W. Mittig, N. Orr, E. Plagnol, C. Ricoaud, Y. Schutz and A.C.C. Villari, J. Phys. G 17 (1991) 463.
[17] Y. Fujita, T. Schwab, J. Schnell, K. Lindmann, H. Wollnik, H. Geissel, B. Fraczak and G. Münzenberg, Adv. Mass Spectrom. 11a (1989) 640.
[18] J. Trötscher, H. Wollnik, K. Balog, H. Eickhoff, B. Franczak, Y. Fujita, H. Geissel, Ch. Klein, K.E.G. Löbner, A. Magel, G. Münzenberg, A. Przewloka, T. Radon, D. Rosenauer, H. Schäfer, M. Sendor, D.J. Vieira, B. Vogel and Th. Winkelmann, Proc. 6th Int. Conf. on Nuclei Far From Stability and 9th Int. Conf. on Atomic Masses and Fundamental Constants, Bernkastel-Kues, Germany, 1992, IOP, Inst. Phys. Conf. Ser. 132 (1993) 959.
[19] H. Geissel, K. Beckert, F. Bosch, H. Eickhoff, B. Franczak, B. Franzke, M. Jung, O. Klepper, R. Moshammer, G. Münzenberg, F. Nickel, F. Nolden, U. Schaaf, C. Scheidenberger, P. Spädtke, M. Steck, K. Sümmerer and A. Magel, Phys. Rev. Lett. 68 (1992) 3412.

[20] J.A. Hipple, H. Sommer and H.A. Thomas, Phys. Rev. 76 (1949) 1877.
[21] G. Graeff, H. Kalinowsky and J. Traut, Z. Phys. A 297 (1980) 35.
[22] P.B. Schwinberg, R.S. Van Dyck, Jr. and H.G. Dehmelt, Phys. Lett. A 81 (1981) 119.
[23] E.A. Cornell, R.M. Weisskopf, K.R. Boyce, R.W. Flanagan, Jr., G.P. Lafatis and D.E. Pritchard, Phys. Rev. Lett. 63 (1989) 1674.
[24] G. Gabrielse, X. Fei, L.A. Orozco, R.L. Tjoelker, J. Haas, H. Kalinowsky, T. Trainer and W. Kells, Phys. Rev. Lett. 65 (1990) 1317.
[25] R.S. Van Dyck, Jr., D.L. Farnham and P.B. Schwinberg, J. Mod. Opt. 39 (1992) 243.
[26] R.S. Van Dyck, Jr., D.L. Farnham and P.B. Schwinberg, Phys. Rev. Lett. 19 (1993) 2888.
[27] Ch. Gerz, D. Wilsdorf and G. Werth, Z. Phys. D 17 (1990) 119.
[28] D. Hagena and G. Werth, Europhys. Lett. 15 (1991) 491.
[29] M.V. Buchanan and R.L. Hettich, Anal. Chem. 65 (1993) 245A.
[30] A.G. Marshall and L. Schweikhard, Int. J. Mass Spectrom. Ion Process. 37 (1992) 118.
[31] G. Bollen, Phys. Scripta, in press.
[32] R.S. Brown and G. Gabrielse, Rev. Mod. Phys. 58 (1986) 233.
[33] G. Bollen, R.B. Moore, G. Savard and H. Stolzenberg, J. Appl. Phys. 68 (1990) 4355.
[34] M. Kretzschmar, Z. Naturforsch. 45a (1990) 965, 979.
[35] M. Kretzschmar, Eur. J. Phys. 12 (1991) 240.
[36] M. Kretzschmar, Proc. Workshop on Physics with Penning Traps, Lertorpet, Sweden, June 1991, eds. G. Bollen and C. Carlberg, Phys. Scripta 46 (1992) 545, 555.
[37] R.S. Van Dyck, F.L. Moore, D.L. Farnham and P.B. Schwinberg, Phys. Rev. A 40 (1989) 6308.
[38] J. Kern, T. Engel, D. Hagena and G. Werth, Proc. Workshop on Physics with Penning Traps, Lertorpet, Sweden, June 1991, eds. G. Bollen and C. Carlberg, Phys. Scripta 45 (1992) 575.
[39] W. Jhe, D. Phillips, L. Haarsma, J. Tanner and G. Gabrielse, Proc. Workshop on Physics with Penning Traps, Lertorpet, Sweden, June 1991, eds. G. Bollen and C. Carlberg, Phys. Scripta 46 (1992) 264.
[40] G. Bollen, H. Hartmann, H.-J. Kluge, M. König, T. Otto, G. Savard and H. Stolzenberg, Proc. Workshop on Physics with Penning Traps, Lertorpet, Sweden, June 1991, eds. G. Bollen and C. Carlberg, Phys. Scripta 46 (1992) 581.
[41] J.B. Jeffries, S.E. Barlow and G.H. Dunn, Int. J. Mass Spectrom. Ion Process. 54 (1983) 169.
[42] D.J. Wineland, W.M. Itano, J.C. Bergquist, J.J. Bollinger and J.D. Prestage, At. Phys. 9 (1985) 3.
[43] G. Bollen, H.-J. Kluge, M. König, T. Otto, G. Savard, H. Stolzenberg, R.B. Moore, G. Rouleau, G. Audi and the ISOLDE Collaboration, Phys. Rev. C 46 (1992) R2140.
[44] G. Gabrielse, W. Jhe, D. Phillips, W. Quint, L. Haarsma, K. Abdullah, H. Kalinowsky and J. Gröbner, Hyperfine Interactions 81(1993) 5.
[45] K. Jungmann, J. Hoffnagle, R.G. DeVoe and R.G. Brewer, Phys. Rev. A 36 (1987) 3451.
[46] D.J. Wineland and H.G.Dehmelt, J. Appl. Phys. 46 (1975) 919.
[47] M. König, G. Bollen, H.-J. Kluge, T. Otto and J. Szerypo, Int. J. Mass Spectrom. Ion Process. 142 (1995) 95.
[48] L. Schweikhard, M. Lindinger and H.-J. Kluge, Int. J. Mass Spectrom. Ion Process. 98 (1990) 25.
[49] L. Schweikhard, Int. J. Mass Spectrom. Ion Process. 107 (1991) 281.
[50] H.G. Dehmelt, Adv. At. Mol. Phys. 5 (1969) 109.
[51] W. Neuhauser, M. Hohenstatt, P. Toschek and H. Dehmelt, Phys. Rev. Lett. 41 (1978) 233.
[52] W.M. Itano and D.J. Wineland, Phys. Rev. A 25 (1982) 35.
[53] D.J. Wineland, W.M. Itano, J.C. Bergquist and R.G. Huelt, Phys. Rev. A 36 (1987) 2220.
[54] D.J. Larson, J.C. Bergquist, J.J. Bollinger, W.M. Itano and D.J. Wineland, Phys. Rev. Lett. 57 (1986) 70.
[55] L.R. Brewer, J.D. Prestage, J.J. Bollinger, W.M. Itano, D.J. Larson and D.J. Wineland, Phys. Rev. A 38 (1988) 859.
[56] G. Gabrielse, X. Fei, L.A. Orozco, R.L. Tjoelker, J. Haas, H. Kalinowsky, T. Trainor and W. Kells, Phys. Rev. Lett. 63 (1989) 1360.
[57] H.G. Dehmelt, Adv. At. Mol. Phys. 3 (1967) 53.
[58] J. André and F. Vedel, J. Phys. 38 (1977) 1381.
[59] H. Schaaf, U. Schmeling and G. Werth, Appl. Phys. 25 (1981) 249.
[60] L.S. Cutler, R.P. Giffard and M.D. McGuire, Appl. Phys. B 36 (1985) 137.
[61] L.S. Cutler, C.A. Flory, R.P. Giffard and M.D. McGuire, Appl. Phys. B 39 (1986) 251.
[62] M.D.N. Lunney, F. Buchinger and R.B. Moore, J. Mod. Opt. 39 (1992) 349.
[63] E.W. McDaniel and E.A. Mason, The Mobility and Diffusion of Ions in Gases (Wiley, New York, 1973).
[64] G. Savard, St. Becker, G. Bollen, H.-J. Kluge, R.B. Moore, Th. Otto, L. Schweikhard, H. Stolzenberg and U. Wiess, Phys. Lett. A 158 (1991) 247.
[65] S. Guan, H.S. Kim, A.G. Marshall, M.C. Wahl, T.D. Wood and X. Xiang, Chem. Rev. 94 (1994) 2161.
[66] ISOLDE Users Guide, ed. H.-J. Kluge, CERN 96-05 (1986).
[67] E. Kugler et al., Nucl. Instr. and Meth. B 70 (1992) 41.
[68] P. Becker, St. Becker, G. Bollen, H.-J. Kluge, G. Savard, W. Stampp and H. Stolzenberg, Vacuum 40 (1989) 495.
[69] S. Becker, G. Bollen, F. Kern, H.-J. Kluge, R. Moore, G. Savard, L. Schweikhard and H. Stolzenberg, Int. J. Mass Spectrom. Ion Process. 99 (1990) 53.
[70] H. Hartmann, Ph.D thesis, Mainz, unpublished.
[71] H. Schnatz, G. Bollen, P. Dabkiewicz, P. Egelhof, F. Kern, H. Kalinowsky, L. Schweikhard, H. Stolzenberg and H.-J. Kluge, Nucl. Instr. and Meth. A 251 (1986) 17.
[72] T. Otto, G. Bollen, G. Savard, L. Schweikhard, H. Stolzenberg, G. Audi, R.B. Moore, G. Rouleau, J. Szerypo, Z. Patyk and the ISOLDE Collaboration, Nucl. Phys. A 567 (1994) 281.
[73] H.-J. Kluge, Phys. Scripta T 22 (1988) 85.
[74] G. Bollen, P. Dabkiewicz, P. Egelhof, T. Hilberath, H. Kalinowsky, F. Kern, H.-J. Kluge, R.B. Moore, H. Schnatz, L. Schweikhard, H. Stolzenberg, G.M. Temmer and G. Ulm, Hyperfine Interactions 38 (1987) 793.
[75] H. Stolzenberg, St. Becker, G. Bollen, F. Kern, H.-J. Kluge, Th. Otto, G. Savard, L. Schweikhard, G. Audi and R.B. Moore, Phys. Rev. Lett. 65 (1990) 3104.
[76] G. Bollen, H.-J. Kluge, Th. Otto, G. Savard, L. Schweikhard, H. Stolzenberg, G. Audi, R.B. Moore, G. Rouleau and the ISOLDE Collaboration, J. Mod. Opt. 39 (1992) 257.
[77] H.-J. Kluge, G. Bollen and C. Carlberg, Proc. on Nuclear Shapes and Nuclear Structure at Low Excitation Energies, Antibes, 1994, in press.
[78] M. König, G. Bollen, H.-J. Kluge, T. Otto, H. Raimbault-Hartmann, G. Savard, E. Schark, L. Schweikhard, H. Stolzenberg, G. Audi, R.B. Moore, G. Rouleau, J. Szerypo, Z. Patyk and the ISOLDE Collaboration, to be submitted to Nucl. Phys. A (1995).
[79] H.W. Ellis, R.Y. Pai, E.W. McDaniel, E.A. Mason and L.A. Viehland, At. Data Nucl. Data Tables 71 (1976) 177.
[80] H.W. Ellis, E.W. McDaniel, D.L. Albritton, L.A. Viehland, S.L. Lin and E.A. Mason, At. Data Nucl. Data Tables 22 (1978) 179.